

1 **Product Ion Distributions using H_3O^+ PTR-ToF-MS: Mechanisms,**
2 **Transmission Effects, and Instrument-to-Instrument Variability**

3 Michael F. Link¹, Megan S. Claflin², Christina E. Cecelski¹, Ayomide A. Akande³, Delaney Kilgour⁴,
4 Paul A. Heine³, Matthew Coggon⁵, Chelsea E. Stockwell⁵, Andrew Jensen^{6,a}, Jie Yu⁷, Han Huynh^{7,b},
5 Jenna C. Ditto^{7,c}, Carsten Warneke⁵, William Dresser⁶, Keighan Gemmell³, Spiro Jorga^{7,d}, Raleigh L.
6 Robertson^{1,e}, Joost de Gouw⁶, Timothy Bertram⁴, Jonathan P.D. Abbatt⁷, Nadine Borduas-Dedekind³,
7 Dustin Poppendieck¹

8 ¹National Institute of Standards and Technology, Gaithersburg, 20899, USA

9 ²Aerodyne Inc., Billerica, 01821, USA

10 ³Department of Chemistry, University of British Columbia, Vancouver, V6T 1Z1, Canada

11 ⁴University of Wisconsin-Madison, Madison, 53706, USA

12 ⁵National Oceanic and Atmospheric Administration, Boulder, 80305, USA

13 ⁶University of Colorado, Boulder, 80309, USA

14 ⁷University of Toronto, Toronto, M5S 3H6, Canada

15 ^aNow at University of Michigan, Ann Arbor, 48109, USA

16 ^bNow at National Oceanic and Atmospheric Administration, Boulder, 80305, USA

17 ^cNow at Washington University in St. Louis, 63130, USA

18 ^dNow at Tofwerk, Thun, 3645, Switzerland

19 ^eNow at University of Colorado, Boulder, 80309, USA

20
21 *Correspondence to:* Michael F. Link (michael.f.link@nist.gov)

22 **Abstract.** Proton-transfer-reaction mass spectrometry (PTR-MS) using hydronium ion (H_3O^+) ionization is widely used for
23 the measurement of volatile organic compounds (VOCs) both indoors and outdoors. H_3O^+ ionization, and associated
24 chemistry in an ion molecule reactor, is known to generate product ion distributions (PIPs) that include other product ions
25 besides the proton-transfer product. We present a method, using gas-chromatography pre-separation, for quantifying PIPs
26 from PTR-MS measurements of nearly 100 VOCs of different functional types including alcohols, ketones, aldehydes, acids,
27 aromatics, organohalides, and alkenes. We characterize instrument configuration effects on PIPs and find that reactor
28 reduced electric field strength (E/N), ion optic voltage gradients, and quadrupole settings have the strongest impact on
29 measured PIPs. Through an interlaboratory comparison of PIPs measured from calibration cylinders we characterized the
30 variability of PIP production from the same model of PTR-MS across seven participating laboratories. Product ion
31 variability was generally smaller (e.g., < 20 %) for ions with larger contributions to the PIPs (e.g., > 0.30), but less
32 predictable for product ions formed through O_2^+ and NO^+ reactions. We present a publicly available library of H_3O^+ PTR-
33 MS PIPs that will be updated periodically with user-provided data for the continued investigation into instrument-to-
34 instrument variability of PIPs.

35 **1 Introduction**

36 Measurements of volatile organic compounds (VOCs) using hydronium ion (H_3O^+) proton-transfer-reaction mass spectrometry
37 (PTR-MS) have become ubiquitous in a variety of applications in the past 25 years (Yuan et al., 2017; Sekimoto and Koss,
38 2021). PTR-MS can measure many VOCs simultaneously with fast ($> 1 \text{ Hz}$) time resolution and low detection limits (e.g., <
39 1 nmol mol^{-1}), and is selective towards VOCs that have a proton-affinity greater than water (e.g., ketones, aldehydes, nitriles,
40 etc.) (De Gouw et al., 2003). However, in the absence of sample pre-separation, isobaric (i.e., same mass-to-charge ratio, m/q)
41 interferences are known to pose challenges to VOC identification and quantification (Coggon et al., 2024; Kilgour et al., 2024;
42 Ditto et al., 2025). Since the early development of PTR-MS, studies have shown that unintended product ions can complicate
43 mass spectra (Warneke et al., 2003; De Gouw and Warneke, 2007), but more recent studies have highlighted ion interferences
44 in measurements of urban air plumes (Coggon et al., 2024) and indoor air (Ernle et al., 2023; Ditto et al., 2025) where
45 interferences are pronounced because VOC concentrations are high and emission sources are diverse. As PTR-MS technology
46 continues to improve through the development of new sample introduction methods, ionization technologies (Krechmer et al.,
47 2018; Breitenlechner et al., 2017; Reinecke et al., 2023), and enhanced mass resolution through the use of time-of-flight mass
48 analyzers, this method will continue to be utilized in concentrated and chemically diverse sample matrices. The popularity of
49 this measurement technique warrants the creation of standardized methods for measuring and quantifying the effects of
50 unintended, or poorly understood, product ion distributions on PTR-MS mass spectra.

51
52 Unintended product ion generation in PTR-MS has been discussed extensively including studies highlighting the importance
53 of VOC fragmentation from H_3O^+ ionization (e.g., aldehydes (Ernle et al., 2023), peroxides (Li et al., 2022), and monoterpenes
54 (Misztal et al., 2012; Kari et al., 2018; Tani, 2013)) and studies using selected-ion flow tube (SIFT) reaction measurements
55 (summarized in a recent review by Hegen et al. (2023)) to differentiate interferences from O_2^+ and NO^+ reagent ion impurities.
56 Pagonis et al. (2019) presented a library of previously reported product ion distributions (PIPs) compiled from measurements
57 of VOCs. However, water cluster contributions to the PIPs were largely not represented in this compilation. The library shows
58 considerable variability in the generation of product ions for a given VOC (e.g., butanal, ethyl acetate, etc.), but from the
59 existing data it is not clear if this variability is explained by instrument operating parameters, features of the specific instrument,
60 or methods of quantifying PIPs.

61

62 In this study we highlight:

63 (1) a gas chromatographic method for measuring PIPs from the ionization of VOCs using PTR-MS (Section 2.2),
64 (2) how instrument configurations can influence PIPs (Section 3.1),
65 (3) instrument-to-instrument variability in measured PIPs determined from an interlaboratory comparison (Section 3.2),
66 (4) the propensity of different VOC functional types to form complex PIPs that include water clusters (Section 3.3),

67 (5) an example of how PIDs can cause ambiguity when identifying ions using a sample of restroom air as a case study (Section
68 3.4),
69 (6) suggestions of how PIDs can be used to aid in identification and quantification of VOCs from PTR-MS mass spectra
70 (Section 3.5),
71 (7) a library of H_3O^+ PTR-MS PIDs available for community use, to be updated with continued collaborative input, and
72 uncertainty estimates (Section 3.6)
73 (8) and recommendations for mitigating and managing unintended product ion generation using PTR-MS (section 3.7).

74 **2 Materials and Methods**

75 **2.1 Product Ion Definitions and Formation Mechanisms**

76 We use observations from previous studies (Koss et al., 2016; Xu et al., 2022; Pagonis et al., 2019; Hegen et al., 2023; Coggon
77 et al., 2024; Li et al., 2024) to identify the reactions, and associated product ions, that are likely to be important from H_3O^+
78 (and impurity NO^+ and O_2^+) ionization of a given VOC. The reaction mechanisms we identify here do not represent an
79 exhaustive accounting of possible product ion formation mechanisms, but instead represent mechanisms most likely to generate
80 the product ions observed from our data. VOCs ($M = \text{VOC}$) with a proton-affinity greater than water (691 kJ mol^{-1}) can undergo
81 a proton-transfer reaction with H_3O^+ to form an H^+ adduct (labelled as MH^+) as described in Reaction 1.



83 Unique from most previous studies, we quantify the contribution of protonated VOC water clusters (labelled as $[\text{MH} \cdot (\text{H}_2\text{O})_n]^+$
84 where $n = 1$ or 2) to the product ion distribution that potentially form from direct association reactions following Reaction 2
85 (Li et al., 2024) and/or termolecular association reactions of a protonated VOC with water vapor following Reaction 3.



88 The presence of a collisional body, B ($B = \text{N}_2$ or O_2), in Reactions 2 and 3 implies a pressure-dependence (Mccrumb and
89 Warneck, 1977; Smith et al., 2020). Direct protonation and water cluster formation can also occur from reaction of VOCs with
90 reagent ion water clusters (De Gouw and Warneke, 2007).



93 However, the addition of the RF-only quadrupole around the IMR (in the instruments evaluated in this study) serves to decrease
94 the influence of higher-order water clusters on ionization chemistry (Krechmer et al., 2018). We note that unlike other PTR-

95 MS instruments, the Vocus PTR-ToF-MS instruments featured in this study have been observed to have ionization chemistry
96 that is not appreciably sensitive to sample water vapor concentrations (Krechmer et al., 2018; Li et al., 2024)..

97 Fragmentation of a protonated VOC can occur from the loss of neutral constituents (e.g., H₂O, CO, and C₂H₄O₂) and/or the
98 dissociation of carbon-carbon bonds (Pagonis et al., 2019). We refer to product ions that result from a fragmentation reaction
99 where water is lost from the protonated VOC, following Reaction 6, as dehydration products (labelled as [MH-H₂O]⁺).



101 We highlight the formation of dehydration products because this type of fragment ion contributed the most to a PID of
102 oxygenated VOCs from our dataset. Because other fragmentation product ions could form through a variety of mechanisms
103 (including from reactions with NO⁺ and O₂⁺), we label other fragmentation product ions as F_n where n = 1,2,3,etc.

104 We highlight two other reaction mechanisms, charge transfer and hydride transfer, that are responsible for generating product
105 ions that often appear in PTR-MS mass spectra. Charge transfer reactions, between a VOC and impurity reagent ions like O₂⁺
106 and NO⁺, can form product ions (labelled as M⁺) that appear in the mass spectrum as ionized VOCs with no changes to
107 elemental composition (Reaction 7).



109 Reactions with NO⁺ can also ionize VOCs via hydride transfer (labelled as [M-H]⁺; Reaction 8) (Koss et al., 2016; Španěl and
110 Smith, 1997).



112 We note that Hegen et al. (2023) recently proposed that product ions appearing in mass spectra as hydride transfer products
113 from reactions with O₂⁺ may actually be charge transfer products that lose a neutral hydrogen atom. For the purposes of this
114 study we classify any product ion that appears in the mass spectrum with the formula [M-H]⁺ as a hydride transfer product.
115 NO⁺ and O₂⁺ ion chemistry can also produce additional product ions through other mechanisms (e.g., hydroxide transfer) not
116 discussed here, but which are summarized in Hegen et al. (2023). We note that in the Vocus instruments used in this study the
117 ratio of NO⁺ and O₂⁺ to H₃O⁺ generated reagent ions cannot be precisely controlled prior to ionization of VOCs in the IMR.

118 We use the above mechanisms for defining the main product ions considered in our analysis and the rules for determining their
119 location in the mass spectrum, relative to the molecular weight (MW) of the VOC, when calculating PIDs (Table 1).

120 **Table 1: Definitions of product ions that occur in PTR-MS mass spectra.**

Product Ion Identity	Product Ion Label	Mass-to-Charge Ratio (Th) ^a
H ⁺ adduct	MH ⁺	MW + 1.007

single water cluster	$[\text{MH}\cdot\text{H}_2\text{O}]^+$	MW + 19.018
double water cluster	$[\text{MH}\cdot(\text{H}_2\text{O})_2]^+$	MW + 37.028
charge transfer	M^+	MW - 0.001
hydride transfer	$[\text{M}-\text{H}]^+$	MW - 1.007
dehydration	$[\text{MH}-\text{H}_2\text{O}]^+$	MW - 18.011
fragment	F_n , n = 1 through 5	variable
other	other	variable

¹²¹ ^aWe express mass-to-charge ratio (m/q) in units of Thomson (Th) which is equal to $1.0364 \times 10^{-8} \text{ kg C}^{-1}$.

¹²² For our analyses we limited the total number of fragment ions that contribute to a PID to five. Most VOCs did not generate
¹²³ more than two fragment ions. Some VOCs (e.g., aromatics generating $\text{C}_6\text{H}_7\text{O}^+$) generated product ions that were consistently
¹²⁴ observed, but we could not easily explain how they formed and so we classify these few ions as “other”.

¹²⁵ 2.2 Method of Quantifying PIDs from GC-PTR-ToF-MS Measurements

¹²⁶ 2.2.1 Measurement of PIDs using Gas Chromatography Proton-Transfer-Reaction Time of Flight Mass Spectrometry ¹²⁷ (GC-PTR-ToF-MS)

¹²⁸ We used gas-chromatography (GC) pre-separation as a technique for isolating VOCs from multi-component standards before
¹²⁹ their measurement by the proton-transfer-reaction time-of-flight mass spectrometer (PTR-ToF-MS) to reduce the influence of
¹³⁰ PIDs from other interfering VOCs. A step-by-step procedure for reproducing this method is presented in the Supplement. PIDs
¹³¹ were measured by our group and collaborating lab partners by first separating target analytes from a VOC mixture using GC
¹³² and then measuring the product ions from H_3O^+ ionization (including ionization by impurity reagent ions O_2^+ and NO^+) of the
¹³³ separated VOC using Time-of-Flight Mass Spectrometry (Claflin et al., 2021; Vermeuel et al., 2023). We discuss the details
¹³⁴ of individual labs’ instrument operation below in Section 2.5. Most of the PIDs for the individual VOCs we report here,
¹³⁵ including measurements from instruments participating in the interlaboratory comparison, were measured from calibration
¹³⁶ cylinders containing multiple VOCs, while Lab 1 measured some PIDs by sampling an air stream of evaporated liquid VOC
¹³⁷ solution. All calibration gas cylinders were less than two years old. VOC sources are listed in the H_3O^+ PID library included
¹³⁸ here as a supplemental document, but also available online (doi: [10.18434/mds2-3582](https://doi.org/10.18434/mds2-3582)). We found that PIDs were difficult to
¹³⁹ quantify from VOCs measured from ambient air samples due to the potential influence of coeluting VOCs on the determination
¹⁴⁰ of the background subtracted mass spectra. However, because of a lack of calibration standards, we included PIDs measured

141 from ambient samples for ethanol and α -pinene measured by Lab 6 as well as a monoterpene acetate ester measured by Lab 1.
142 Sample concentrations varied depending on cylinder or liquid solution concentrations, but target VOC concentrations were
143 always less than 10 nmol mol⁻¹.

144
145 All the data presented in this manuscript were collected on the “Lab 1” PTR-ToF-MS, unless otherwise noted such as in Section
146 3.2 where we compare PIDs measured from different instruments. We differentiate between the seven different laboratories
147 that contributed data by labelling the data as coming from Labs 1 through 7 (e.g., “Lab 1”). Each instrument used a GC for
148 pre-separation of VOC mixtures and a Vocus Time-of-Flight Mass Spectrometer with H₃O⁺ ionization for subsequent
149 measurement of PIDs. In principle, the chemistry discussed here applies to all PTR-MS instruments that use H₃O⁺ chemical
150 ionization, but differences in ionization technology, ion transfer optics, and mass analyzers between instruments may have
151 instrument-specific effects on PID measurements. Limited evidence suggests that the PIDs resulting from fragmentation in the
152 Vocus PTR-ToF-MS, as used in this study, and a PTR-MS using a drift tube (instead of an ion-molecule reactor) are
153 comparable (Krechmer et al., 2018), but we limit the implications of our measurements to Vocus PTR-ToF-MS (Tofwerk)
154 instruments until future studies comparing PIDs from different PTR-MS instruments can be performed. The mass spectrometer
155 for Lab 5 used a modified version of the Vocus ionization source (Gkatzelis et al., 2024; Coggon et al., 2024) and the mass
156 spectrometer for Labs 4 and 5 had a lower mass resolution compared to the other instruments (approximately 4000 versus
157 10000 full-width half-maximum, respectively). Lab 5 also used a custom-built GC whereas all the other instruments used a
158 commercially available GC (Aerodyne Research). Because the principle of operation was similar for all instruments, we
159 describe in more detail below the operation of the Lab 1 instrument. Operating details for each of the instruments in the
160 interlaboratory comparison are included in the H₃O⁺ PID library (also outlined in Table 2).

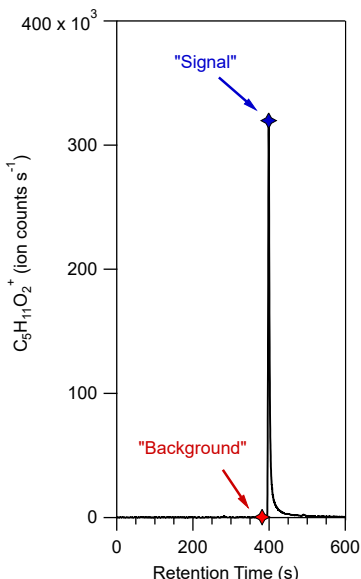
161
162 We describe the GC sampling method used for Lab 1 below but note that operational differences may have been utilized for
163 the different labs represented in the interlaboratory comparison (e.g., temperatures and make-up flow rates). Analytes from
164 multi-component VOC samples were first collected using thermal desorption preconcentration ahead of the chromatographic
165 separation before ionization by the PTR-ToF-MS. For the laboratories that utilized the commercial GC systems, sample air
166 was passed at a rate of 100 cm³ min⁻¹ over a multibed sorbent tube (containing Tenax TA, Graphitized Carbon, and Carboxen
167 1000) where VOCs were collected for 10 minutes. The VOCs were then desorbed from the sorbent tube and collected onto a
168 second preconcentration stage, a focusing trap. VOCs were then rapidly desorbed from the focusing trap and injected on a
169 mid-polarity column (Restek MXT-624, 30 m \times 0.25 mm \times 1.4 μ m). VOCs were separated with a helium carrier gas flow of
170 2 cm³ min⁻¹ during the temperature programmed chromatographic separation. Analyte eluting from the column passed through
171 a transfer line, heated to 100 °C, and was combined with 150 cm³ min⁻¹ of ultra pure zero air before being sampled by the
172 PTR-ToF-MS. Chromatograms were collected over 10 minutes. Versions of the GC system used in this study are described in
173 detail elsewhere (Claflin et al., 2021; Vermeuel et al., 2023; Jensen et al., 2023).

175 The PTR-ToF-MS sampled the diluted GC eluent/zero air mixture at a rate of $120 \text{ cm}^3 \text{ min}^{-1}$ through a polyether-ether-ketone
176 (PEEK) capillary (25 mm, 0.25 mm ID) which directs the flow to the center of the focusing ion-molecule reactor (IMR). A
177 separate flow of water vapor saturated air enters a pre-chamber where a plasma creates a reagent ion distribution that includes
178 H_3O^+ , water adducts (i.e., $\text{H}_3\text{O}(\text{H}_2\text{O})_n^+$ where $n = 1,2,3,\text{etc.}$), as well some amount of O_2^+ and NO^+ reagent ions that are
179 considered impurities. These reagent ions from the pre-chamber enter the IMR alongside the eluent sample flow. There are
180 two features of the Vocus PTR-ToF-MS discussed thus far that distinguish this instrument from other instruments that use
181 H_3O^+ chemical ionization: (1) the Vocus PTR-ToF-MS uses a radio frequency (RF) only quadrupole around the IMR to
182 generate H_3O^+ ions in excess by declustering water adducts of H_3O^+ and (2) the water vapor concentration in the IMR is
183 estimated to be approximately 20 % by volume (Krechmer et al., 2018). We do not discuss the effects of IMR quadrupole
184 voltage settings on PIDs here, but instead point the reader to Li et al. (2024) for more information. We do not expect the
185 differences in IMR quadrupole settings utilized in this study to explain the differences observed in the interlaboratory PID
186 comparisons. The higher water vapor concentrations in the Vocus IMR are likely to have impacts that are unique to the Vocus
187 PTR-ToF-MS for PIDs from VOCs historically affected by a water-vapor dependence (e.g., formaldehyde, hydrogen cyanide,
188 and formic acid) compared to PTR-MS instruments using a drift tube where water vapor concentrations are lower.

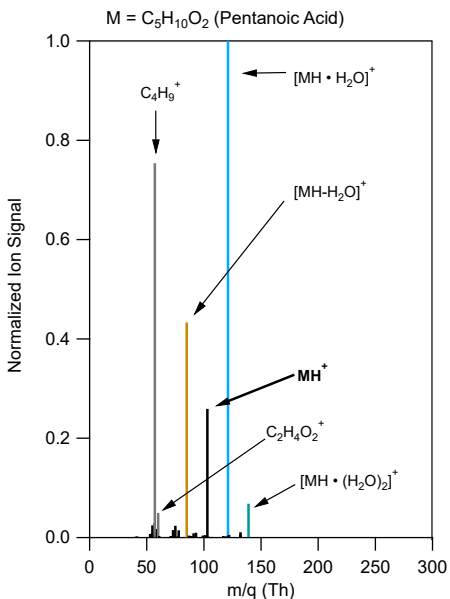
189 **2.2.2 PID Quantification from GC-PTR-ToF-MS Measurements**

190 For our method of quantifying PIDs, we use chromatographic separation prior to detection of product ions with PTR-ToF-MS.
191 The advantage of using a GC when quantifying PIDs is that analytes in multi-component mixtures (e.g., calibration standards
192 or ambient samples) can be separated before detection and thus avoid interference with PID quantification.
193 Fig. 1 shows an example, using pentanoic acid, of the chromatographic method of determining PIDs from GC-PTR-ToF-MS
194 measurements.

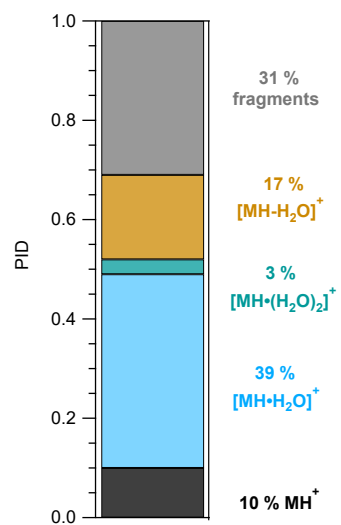
(a) Selected Ion Chromatogram



(b) Isolated Mass Spectrum



(c) Product Ion Distribution



195

196 **Figure 1: Steps of a method for determining PIDs using pentanoic acid as an example.** (a) The selected ion chromatogram for the
 197 expected H^+ adduct of pentanoic acid, $C_5H_{11}O_2^+$, showing ion signal as a function of retention time. Markers show the retention time
 198 when the maximum signal (blue) and background (red) mass spectra were defined. (b) The pentanoic acid isolated mass spectrum is
 199 determined by subtracting the background mass spectrum from the maximum signal mass spectrum. Ion signals are normalized to the highest ion signal. (c) Product ion distribution (PID) measured from the isolated mass spectrum for pentanoic acid using data
 200 from (b).

201

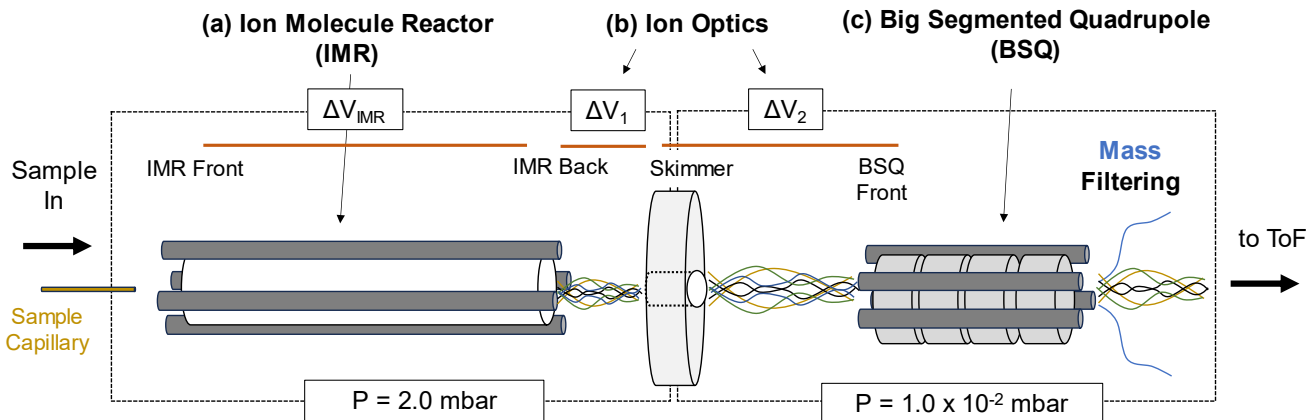
202 As shown in Fig. 1a, we use a selected ion chromatogram from the expected H^+ adduct ion signal to determine where to define
 203 the background and maximum signal mass spectra. The background mass spectrum is subtracted from the signal mass spectrum
 204 to create the isolated mass spectrum shown in Fig. 1b. The high-resolution fitted peak areas of each product ion m/q , with at
 205 least 1 % contribution to the isolated mass spectrum, are added together to represent the sum product ion signal and the relative
 206 contribution of each ion to the sum represents the PID. As shown in Figure 1b, some analytes had ions that made small
 207 contributions (< 5 %) to the isolated mass spectrum in addition to the ions that were included in the PID for pentanoic acid. If
 208 ions could not reasonably be explained mechanistically as product ions from the target analyte and made small contributions
 209 (< 5 %) to the isolated mass spectrum we omitted them in the determination of a PID.

210

2.3 PID Measurement as a Function of Instrument Settings

211

In the PTR-ToF-MS instruments in this study, chemistry that forms PIDs occurs in the IMR immediately downstream of the
 212 capillary that serves as the sample inlet for the instrument (Fig. 2).



215 **Figure 2: Simplified diagram of the front end of the PTR-ToF-MS evaluated in this study.** Sample air enters the instrument through
 216 a capillary and is directed to the IMR. (a) The IMR voltage difference between the back and front (ΔV_{IMR}) in part controls the
 217 energy of ion collisions. (b) After the IMR, there are two sections of the ion trajectory with voltage differentials that occur at
 218 relatively high pressures, these are between the transfer optics (Skimmer – IMR back; ΔV_1 and BSQ front – Skimmer; ΔV_2) as
 219 shown. (c) The big segmented quadrupole (BSQ) is an RF-only quadrupole that filters ions acting as a high-pass filter. Pressures for
 220 the regions defined by the boxed areas are shown at the bottom of the figure (1 mbar = 100 Pa).

222 In the IMR a voltage differential (ΔV_{IMR} in Fig. 2) creates an electric field that focuses ions through the reactor. However, the
 223 electric field (E , $V m^{-1}$) strength the ions experience is reduced by the reactor air number density (N , $molecules cm^{-3}$). The
 224 influence of the reduced electric field strength, E/N , on H_3O^+ ion chemistry is well-documented in PTR-MS literature for both
 225 drift tube (Yuan et al., 2017) and ion-molecule reactors (Krechmer et al., 2018) and can be calculated following Eq. 1 (De
 226 Gouw and Warneke, 2007):

$$227 \frac{E}{N} = \frac{\Delta V_{IMR} \cdot T \cdot R}{L_{IMR} \cdot P \cdot A_v \cdot 10^{-21}} \quad (1)$$

228 where ΔV_{IMR} is the voltage differential between the IMR back and front (V), T is the IMR temperature (K), R is the ideal gas
 229 constant ($8.3 \times 10^{-2} m^3 kPa K^{-1} mol^{-1}$), L_{IMR} is the length of the IMR (10 cm for the instruments in this study), P is the IMR
 230 pressure (kPa), A_v is Avogadro's number, and 10^{-21} is a conversion factor from $V m^{-2}$ to the unit of Townsend (Td). We note
 231 that for the Vocus instruments discussed here the RF-only quadrupole around the IMR adds to the electric field strength, an
 232 effect that is not accounted for in this equation. Li et al. (2024) showed that although the IMR RF voltage can affect analyte
 233 sensitivity it did not affect PIDs. All the instruments in this study operated with similar RF voltages for the IMR (between 400
 234 V and 450 V) so we exclude this contribution from the E/N values we report. To measure the effects of E/N on select PIDs in
 235 this study, we varied the pressure in the IMR—while keeping the reactor voltage differential (ΔV_{IMR}) constant—between 1.4
 236 mbar (0.14 kPa) and 3.0 mbar (0.30 kPa) resulting in E/N values ranging from 90 Td to 190 Td.

238 Although PIDs are initially formed in the IMR, m/q-dependent transmission efficiencies between the IMR and the time-of-
239 flight mass analyzer can affect the PIDs that are ultimately measured (Jensen et al., 2023; Li et al., 2024). We isolate three
240 parts of the ion trajectory in the instrument as possible locations for affecting PIDs through collisional dissociation, quadrupole
241 mass filtering, and/or other transmission effects. The first two areas where ions may undergo declustering of water adducts or
242 collisionally induced fragmentation are shown in Fig. 2 as ΔV_1 and ΔV_2 , which correspond to the voltage differential between
243 the Skimmer and IMR back (ΔV_1) and the BSQ front and Skimmer (ΔV_2). These ion optic voltage differences have been
244 demonstrated to contribute to declustering reactions in a similar mass spectrometer (Brophy and Farmer, 2016).

245
246 In this study, we vary the voltage difference between each ion optic component relationship following the methodology of
247 previous studies (Brophy and Farmer, 2016; Lopez-Hilfiker et al., 2016) by incrementally changing the entire set of voltages
248 upstream (i.e., in the direction of the inlet) of the tested component relationship. We performed these ensemble voltage changes
249 manually without the use of tuning software. The range of tested voltages are based on the observed voltage differences in the
250 interlaboratory comparison dataset. For ΔV_1 we measured PIDs as a function of ΔV ranging from -3 V to -50 V and for ΔV_2
251 we tested a range of -1 V to -10 V. We performed these PID sensitivity tests to instrument configuration only on the instrument
252 corresponding to Lab 1. The skimmer component in the ΔV_1 and ΔV_2 relationships described here corresponds to the skimmer
253 located right before the BSQ (i.e., not the “skimmer 2” component also present in all versions of the Vocus instrument
254 evaluated here.)

255
256 The third ion optic component we evaluate is the effect of the RF-amplitude voltage of the big segmented quadrupole (BSQ)
257 in filtering ions of different m/q. The primary function of the BSQ is to act as a high-pass filter limiting the transmission of
258 lower-mass reagent ions (i.e., H_3O^+ m/q = 19.02 Th and $(H_2O)H_3O^+$ m/q = 37.03 Th) to the detector and thus extending the
259 lifetime of the detector (Krechmer et al., 2018). Product ions with an m/q in the range of these major reagent ions will also
260 experience decreased transmission (Jensen et al., 2023; Li et al., 2024). We measured PIDs at nine different BSQ voltage
261 settings between 225 V and 450 V. Although we focus on three areas where ion m/q dependent transmission effects may
262 occur, we note that mass discrimination effects can occur elsewhere in the instrument and for other reasons such as detector
263 degradation (Heinritzi et al., 2016) or discrimination of higher m/q ions because of other quadrupole transmission effects
264 (Holzinger et al., 2019; Antony Joseph et al., 2018).

265 **2.4 PID Measurement as a Function of Sample Capillary Insertion Distance**

266 A small PEEK (25 mm length, 0.18 mm inner diameter) capillary, secured by two Viton o-rings, serves as the sample inlet to
267 the instrument. The distance that this capillary is inserted into the instrument can be manually changed and impacts the
268 ionization chemistry that occurs immediately at the exhausting end of the capillary. We characterized the effects of the capillary
269 insertion distance on the measured PID from pentanoic acid by turning off all voltages to the IMR, closing the standby valve
270 between the IMR region and the rest of the instrument, and manually adjusting the capillary to a different insertion distance.

271 With the capillary at the desired insertion distance, we returned the IMR to standard operating conditions and acquired a GC
272 measurement of pentanoic acid. We then changed the capillary insertion distance between 3 mm and 13 mm for five total
273 measurements.

274 **2.5 Interlaboratory Comparison of PIDs**

275 We compare PIDs from seven different instruments under lab-defined settings. Lab-defined settings for all instruments are
276 shown in Table 2.

Table 2. Lab-defined instrument settings for datasets contributed by each lab. Some labs provided data where the instrument was operated under different settings, and/or data was collected years apart, and thus we differentiate datasets by the letters a, b, and c.

ID	IMR T (°C)	IMR P (mbar) ³	ΔV _{IMR} (V)	E/N (Td)	BSQ RF Voltage (V)	ΔV ₁ (V)	ΔV ₂ (V)	Water Flow (scm ³ min ⁻¹) ⁴	Inlet Flow (cm ³ min ⁻¹)	Date Acquired
Lab1a	60	2.0	580	133	350	-22.5	-4.1	20	120	5/2023
Lab1b	60	2.0	580	133	300	-22.5	-4.1	20	120	5/2024
Lab 2a ¹	60	2.4	575	110	300	-29.0	-7.3	19	100	10/2020
Lab 2b ^{1,2}	60	2.4	660	126	400	-4.4	-8.1	20	100	11/2023
Lab 3a ²	100	1.5	365	125	215	-39.7	-4.5	20	96	12/2020
Lab 3b ²	100	1.5	385	133	215	-32.0	-4.0	15	88	11/2022
Lab 4	100	2.5	450	122	320	-40.5	-5.1	20	79	9/2024
Lab 5 ²	110	2.5	624	131	250	-27.5	-3.5	21	180	7/2021
Lab 6a ²	90	1.5	480	160	255	-19.1	-6.5	15	260	3/2021
Lab 6b ²	90	1.5	480	160	255	-19.1	-6.5	15	290	5/2022
Lab 7a	100	2.2	570	133	325	-39	-4.2	20	100	4/2022
Lab 7b	100	2.2	570	133	325	-39	-4.2	20	100	9/2022
Lab 7c	100	2.2	570	133	325	-39	-4.2	15	100	5/2023

279¹Lab 2a and Lab 2b data comes from two different instruments.280²IMR quadrupole RF voltage was 400 V. The IMR quadrupole RF voltage was 450 V for other instruments.281³1 mbar = 100 Pa.282⁴Standard cm³ min⁻¹ (standard conditions = 293.15 K and 101.325 kPa)283 **2.6 Restroom Air Measurement**284 To demonstrate the uncertainties introduced by interfering product ions in ambient air, we deployed our GC-PTR-ToF-MS to
285 a restroom as detailed in Link et al. (2024). Briefly, the restroom air sample was acquired during a weekend-long measurement
286 period. The restroom air contained elevated concentrations of terpenoids (i.e., monoterpenes, monoterpenic alcohols, and

287 monoterpane acetate esters) that reacted with ozone and created oxygenated VOC products. The relative VOC composition of
288 the restroom air stayed consistent over the measurement period with concentrations decreasing from the start of the period to
289 the end. We highlight one GC chromatogram acquired during that measurement period to demonstrate the effect of PIDs on
290 ion attribution from an indoor air sample.

291 **2.7 Data Processing**

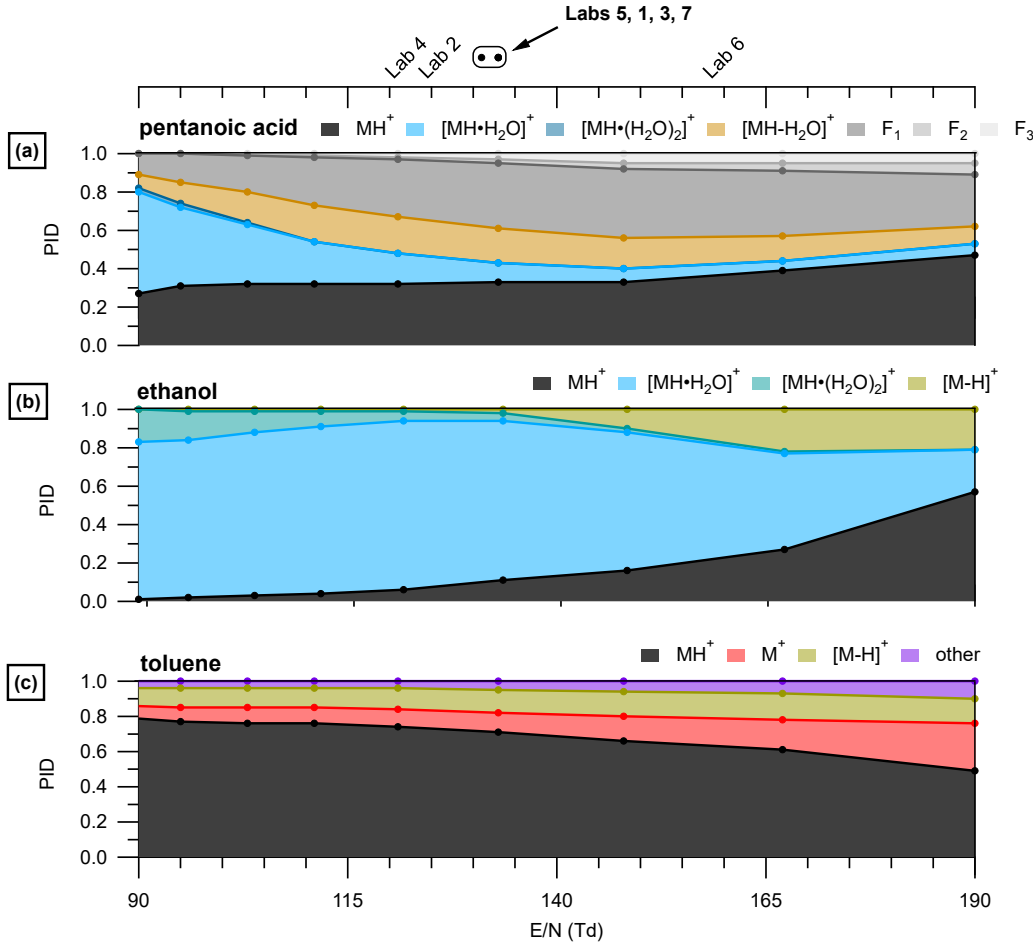
292 During GC measurements mass spectra were collected at a rate of 5 Hz. Mass calibration, resolution and average peak shape
293 determination, and high-resolution peak fitting were all performed in Tofware v3.2.5 (Aerodyne Research). Mass accuracy
294 was maintained within ± 6 ppm when performing mass calibrations. A peak list containing 1046 ions was used for high-
295 resolution peak fitting. VOCs present in calibration standards were used to inform what product ions were likely to be expected
296 following the definitions in Table 1. Selected ion chromatograms and isolated mass spectra were produced using the analysis
297 tools in TERN v2.2.20 software (Aerodyne Research). Ion signals were not ToF duty cycle corrected.

298 **3 Results and Discussion**

299 **3.1 Influence of Instrument Configuration on PIDs**

300 **3.1.1 Influence of IMR E/N on PIDs**

301 IMR E/N is an important determinant of water clustering and fragmentation. Fig. 3 shows the PID for pentanoic acid, ethanol,
302 and toluene measured at different E/N values.



303
304 **Figure 3: (a) Pentanoic acid PID as a function of E/N. Colored text in the legend above the panel correspond to the colored traces in**
305 **306 E/N values used by the different labs in the interlaboratory comparison**
307 **308 are shown in the top axis. The circle markers indicate values where the lab text markers would overlap and are listed in order of**
309 **310 E/N in the corresponding text label. Measurements were acquired with a BSQ voltage of 300 V.**

311 We highlight pentanoic acid because it forms fragments and water clusters across a wide m/q range (m/q 39.02 to m/q 139.10).
312 We highlight ethanol because it forms water clusters and a hydride transfer product. We highlight toluene because it forms
313 charge and hydride transfer products as well as a product we classify as “other” (C₆H₇O⁺). In the case of pentanoic acid, the
314 contribution of the H⁺ adduct increased from 0.26 to 0.47 with increasing E/N (Figure 3). This change in the H⁺ adduct
315 contribution was mostly due to the decreasing contribution of the first water cluster from 0.53 at the lowest E/N to 0.06 at the
316 highest E/N. In contrast, the contribution of total fragmentation products (dehydration + other fragment ions) increased from
317 0.20 at the lowest E/N to 0.60 at an E/N of 148 Td (Figure 3). Above E/N 148 Td, the contribution of the H⁺ adduct to the PID
increases and the relative contribution of fragment ions decreases. The general pattern of water cluster and fragment product
ion variation with E/N shown in Fig. 3 suggests lower E/N will decrease the contributions of fragment ions in the mass

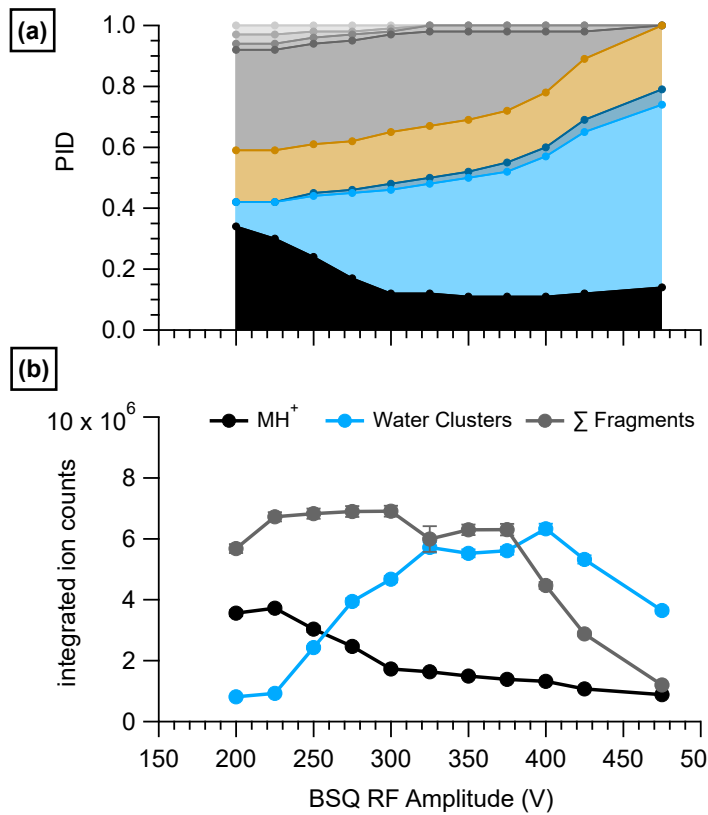
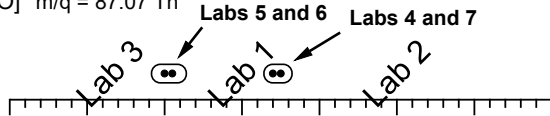
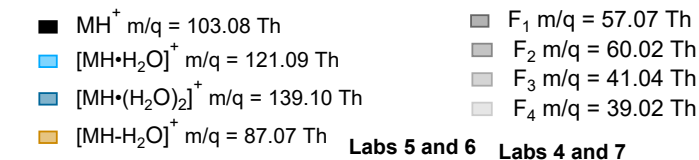
318 spectrum. However, higher E/N values will decrease the contribution of water clusters to the mass spectrum. Because different
319 PIDs (i.e., different contributions of fragments, water clusters, and the H⁺ adduct) are generated at the different values of E/N
320 tested here, measurable product ion formation will likely occur for a variety of VOCs regardless of E/N. As is the case for the
321 three VOCs highlighted here, secondary product ion generation is not suppressed across the tested E/N range.

322
323 As another example, we show (Fig. 3b and 3c) how the PIDs vary as a function of E/N for species that can generate product
324 ions from reactions with impurity reagents NO⁺ and O₂⁺. Impurity reagent ions are generated unintentionally in the PTR-ToF-
325 MS and result from oxygen ionizing in the ion source plasma. We show here, using ethanol and toluene as examples, that
326 higher E/N may qualitatively indicate that a user could expect more important contributions of hydride and charge transfer
327 products to the PID. Ethanol forms C₂H₅O⁺, a likely hydride transfer product from reaction with NO⁺, while toluene forms
328 C₇H₇⁺, a likely hydride transfer product from reaction with NO⁺ (Smith et al., 2020), and C₇H₈⁺, a charge transfer product from
329 reaction with both O₂⁺ and NO⁺ (Coggon et al., 2024; Koss et al., 2016). The increased contributions of charge and hydride
330 transfer products to the PIDs of ethanol and toluene potentially suggest an increased influence of impurity reagent ions, but
331 we do not have an explanation for how impurity reagent ion concentrations would increase with increasing E/N in the IMR.
332 We note that the presence of air leaks in the reagent delivery system may increase the importance of impurity reagent ion
333 chemistry. Also, purging the water reagent source with pure nitrogen may be a possible method to decrease impurity reagent
334 ion chemistry due to the presence of dissolved oxygen.

335 **3.1.2 Influence of BSQ RF Voltage on PIDs**

336 Another important influence on PIDs is the BSQ RF amplitude voltage (referred to hereafter as “BSQ voltage”). BSQ voltages
337 observed from the lab-defined settings in the interlaboratory comparison dataset ranged from 215 V to 400 V. The BSQ acts
338 as a high-pass filter and thus low-mass ion transmission decreases with increasing BSQ voltage. In other words, at low BSQ
339 voltages (e.g., 225 V) we would expect to see greater transmission of low-mass ions (e.g., m/q < 55.04 Th) compared to higher
340 voltages (e.g., 450 V). When considering how the BSQ affects PIDs we expected that product ions that were low-mass, both
341 H⁺ adduct and fragment ions, would be most affected by different BSQ voltages versus the higher m/q water cluster products.

342
343 Fig. 4 shows the ion signals and PIDs for pentanoic acid measured across a range of BSQ voltages at an E/N of 133 Td.



344

345 Figure 4: Pentanoic acid (a) PID and (b) product ion signals as a function of BSQ RF Amplitude voltage measured with IMR E/N =
 346 133 Td. Because the BSQ is supposed to mainly act as a high pass filter, the m/q values for the product ions are listed next to the
 347 product ion definition in the legend to contextualize m/q-dependent transmission effects from the changing BSQ voltage. The ion
 348 signals for the MH^+ ion, sum of the water cluster product ions, and sum of the fragment product ions were determined by integrating
 349 product ion peaks from their selected ion chromatograms. Error bars are difficult to visualize but show the error from the residual
 350 peak area. The BSQ voltages used by the laboratories in the comparison are shown in the top axis. The circle markers indicate values
 351 where the lab text markers would overlap and are listed in order of BSQ voltage in the corresponding text label.
 352

353 The integrated ion counts in Fig. 4 demonstrate the effect of the BSQ voltage on total transmission of ions whereas the PIDs
 354 demonstrate transmission effects relative to other ions. Because the BSQ mainly acts as a high-pass filter, BSQ effects on PIDs
 355 are likely to be most pronounced for VOCs that generate lower m/q ions like the fragment ions generated from pentanoic acid.
 356 The contribution of fragment ions to the PID for pentanoic acid are most pronounced at BSQ voltages less than 350 V. As the

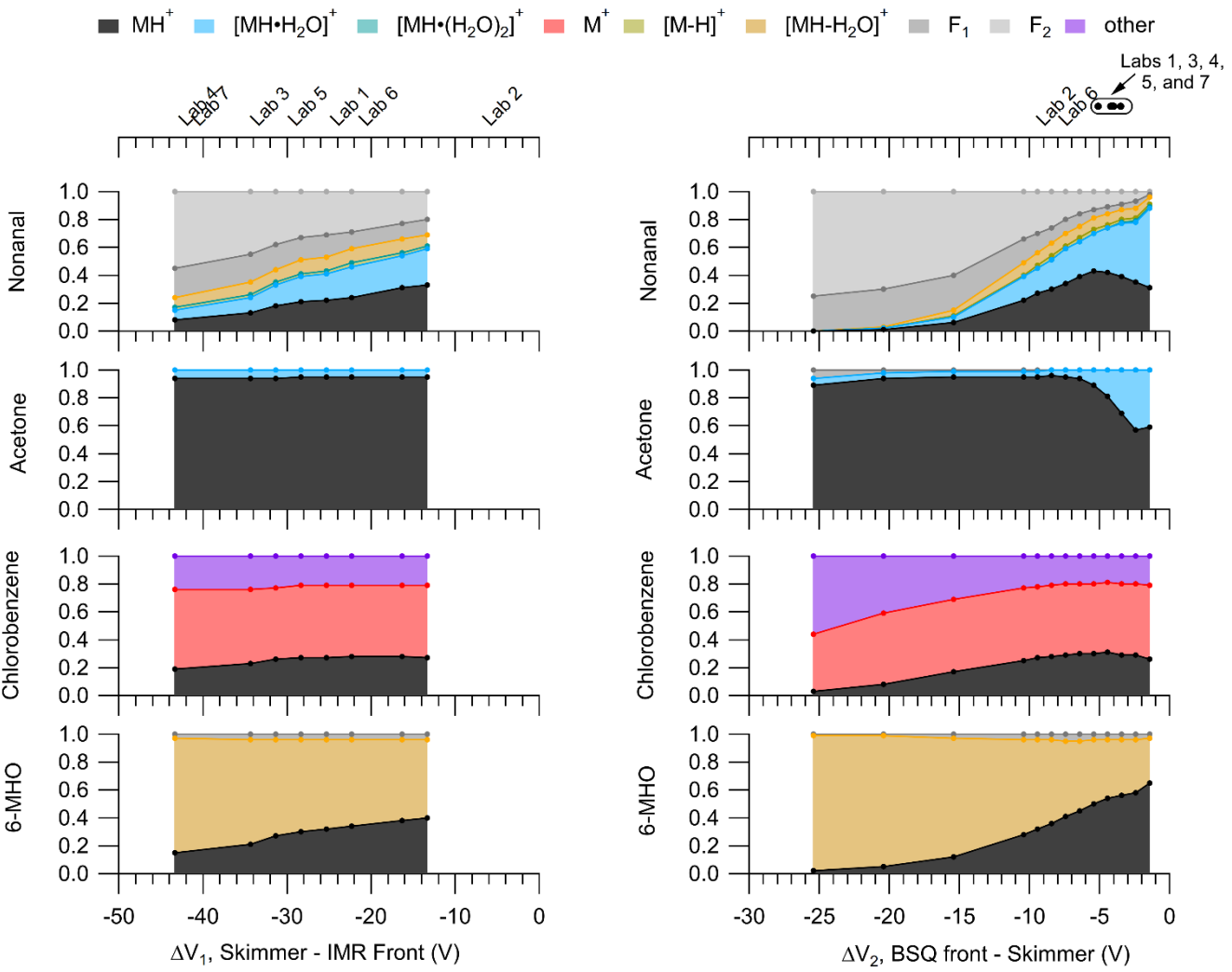
357 BSQ voltage increases, the lowest m/q product ion ($C_3H_5^+$, $C_3H_5^+$, $C_4H_9^+$, and $C_2H_4O_2^+$) contributions decrease. At 450 V the
358 $C_3H_3^+$ and $C_3H_5^+$ ions no longer make measurable contributions to the PID and the contribution of $C_4H_9^+$ has decreased by a
359 factor of five. However, as the contribution of lower m/q ions to the PID decreases with increasing BSQ voltage the
360 contribution of higher m/q ions (H^+ adduct and water clusters) generally increase for pentanoic acid. The relative contribution
361 of the single water cluster to the PID increases by a factor of six at 450 V compared to 225 V. Notably, we cannot explain why
362 the integrated ion counts for the MH^+ ion from pentanoic acid decrease going from a BSQ voltage of 200 V to 300 V.

363 **3.1.3 Influence of Ion Optic Voltages and Capillary Distance on PIDs**

364 We found that ion optic voltage differences (i.e., ΔV_1 and ΔV_2 in Figure 2) and the capillary insertion distance did not impact
365 the pentanoic acid PID as clearly as E/N and the BSQ settings. Figures presented in the Supplement demonstrate the variability
366 in PIDs measured for pentanoic acid when testing the voltage differences for ΔV_1 (Fig. S2) and ΔV_2 (Fig. S3), and the sample
367 capillary insertion distance (Fig. S5). We also analyzed the PID for benzene to investigate if charge transfer product ions were
368 modulated by the capillary distance. We did not observe any clear trends in the PID for pentanoic acid or the charge transfer
369 product ion contributions to the benzene PID as a function of capillary distance.

370

371 Although we did not observe major effects of ΔV_1 and ΔV_2 on the pentanoic acid PID, we did observe notable changes in the
372 PIDs for other VOCs as shown in Fig. 5.



373
 374 **Figure 5: PIDs for nonanal, acetone, chlorobenzene, and 6-methyl-5-heptene-2-one (6-MHO) as a function of ΔV_1 (left) and ΔV_2 (right).** The top axes for both left and right panels correspond to the bottom axes and the midpoint of the labels show the ΔV corresponding to the respective lab. Circle markers on the top right axis correspond to a range of ΔV of ± 1 V and the text labels shown above for clarity. These PIDs were measured at an IMR E/N of 150 Td and a BSQ voltage of 300 V. Fig. S4 in the Supplement shows these PIDs measured at an IMR E/N of 106 Td.

380 Changes in PIDs induced by voltage gradients across the ion optics likely result from collisionally assisted fragmentation and
 381 declustering.. As shown in Fig. 5 we observe increased fragmentation and increased water adduct declustering as the absolute
 382 ΔV increases for both ΔV_1 and ΔV_2 . These changes in the PIDs are associated with the increased energy of ion collisions as
 383 they traverse the voltage gradient. These collisional effects are highlighted in the PIDs for nonanal and 6-MHO where
 384 fragmentation product ion contributions to the PIDs increase with increasing ΔV .

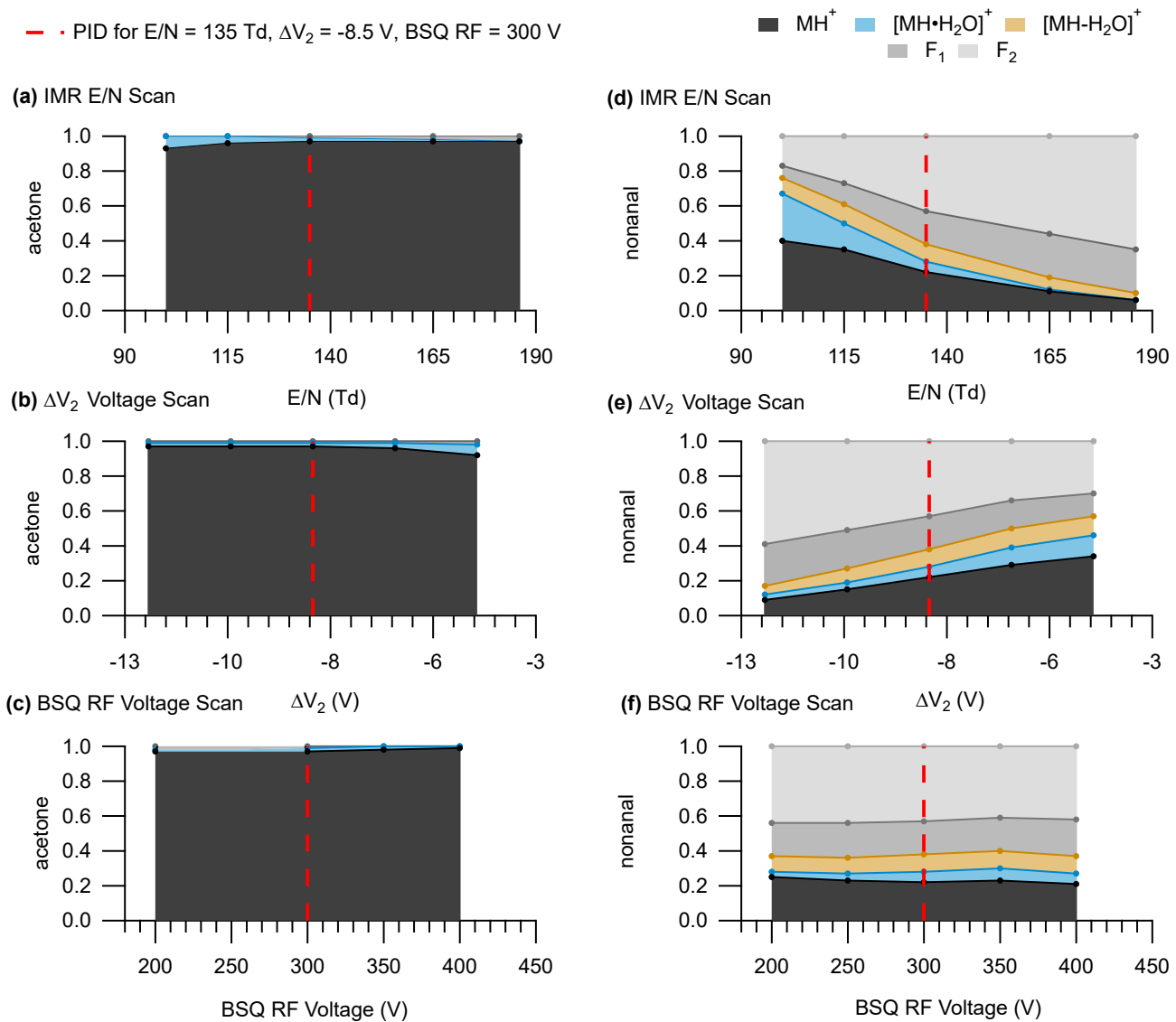
385 The PID for chlorobenzene consists of the H^+ adduct, a charge transfer product, and another product ion formed by an unknown
386 mechanism, $\text{C}_6\text{H}_7\text{O}^+$. Compared to nonanal and 6-MHO the PID for chlorobenzene does not show as strong of an influence of
387 ion collisions changing the PID. The relative stability of the chlorobenzene PID with ΔV for both ΔV_1 and ΔV_2 suggests that
388 other species that have PIDs mostly containing charge transfer and hydride transfer product ions may also be minimally
389 influenced by ion optic voltage differences. However, the increasing contributions of both $\text{C}_6\text{H}_7\text{O}^+$ (the “other” product ion)
390 and $\text{C}_6\text{H}_5\text{Cl}^+$ (the charge transfer product ion) to the chlorobenzene PID with increasing ΔV_2 possibly suggest collisions may
391 be important for converting the H^+ adduct to these other product ions given high enough collisional energy.
392

393 We did not observe major effects of ion optic voltage differences on the pentanoic acid PID, but the results in Fig. 5 suggest
394 that increased ion optic voltage differences may increase the contribution of fragmentation and decrease the contribution of
395 water cluster ions to a PID for other molecules. The voltage differences used by the different labs included in the interlaboratory
396 comparison encompassed a smaller range for ΔV_2 compared to ΔV_1 .
397

398 We observe sensitive changes to the nonanal and 6-MHO PIDs within the narrow range of voltages used for ΔV_2 , but also
399 measurable, albeit less sensitive, changes in the PIDs for ΔV_1 . Although the effects of ΔV_1 on PIDs was not as sensitive as
400 ΔV_2 we acknowledge the potentially important role this ion optic voltage difference could have in interpreting differences in
401 PIDs measured between labs such as Labs 4 and 6, in the interlaboratory comparison, which have a difference in ΔV_1 between
402 the two labs of approximately 20 V. For instance, going from the highest measured ΔV_1 we measured for 6-MHO to the lowest
403 ΔV_1 , the contribution of the MH^+ product ion to the PID decreases by 30 % (i.e., from 0.59 to 0.36). Because of the greater
404 sensitivity of the PIDs to ΔV_2 , we highlight the importance of this relationship in affecting PIDs but note that Fig. 5
405 demonstrates that differences in ΔV_1 are likely important enough to create differences in product ion contributions to PIDs on
406 the order of 10 % to 30 % for the instruments evaluated as part of the interlaboratory comparison.
407

408 An important implication of sensitive declustering and fragmentation effects from ΔV_2 is that the IMR E/N alone cannot
409 accurately predict the extent of possible fragmentation or declustering affecting PIDs. We show in Fig. 6, how the PID for
410 acetone and nonanal changes when varying the IMR E/N, ΔV_2 , and BSQ voltage individually compared to a reference set of
411 instrument operating parameters (red dotted line corresponding to $\text{E/N} = 135 \text{ Td}$, $\Delta V_2 = -8.5 \text{ V}$, and BSQ RF voltage = 300
412 V). For both acetone and nonanal, we see the same effects of increasing water cluster declustering and fragment ion formation
413 as E/N goes from low to high values (Fig. 6a and 6d) as we observed for pentanoic acid (Fig. 3). While keeping the IMR E/N
414 = 135 Td and varying ΔV_2 we see changes in the nonanal PID (Fig. 6e) that are nearly as pronounced as similar incremental
415 changes in the IMR E/N. For instance, at a $\Delta V_2 = -4.4 \text{ V}$ the PID for nonanal is similar to the PID measured at 100 Td. To a
416 rough approximation, a 1 V change in ΔV_2 is equivalent to a change in IMR E/N of 9 Td for nonanal. A similar sensitivity to
417 ΔV_2 is observed for acetone, but our interpretation is limited because the PID only has a minor contribution from the water
418

419 cluster under all conditions. In contrast to pentanoic acid (Fig. 4), major PID changes for acetone and nonanal were not
 420 observed when scanning the BSQ RF voltage demonstrating that the combined influence of the instrument components
 421 evaluated here on measured PIDs can vary considerably between different chemical species.



422
 423 **Figure 6: PIDs for acetone (left panels) and nonanal (right panels). Panels a and d show PIDs as a function of IMR E/N, panels b**

424 and e show PIDs as function of ΔV_2 , and panels c and f show PIDs as a function of BSQ RF voltage. The red dotted line

425 shows where the settings for the IMR, ΔV_2 , and the BSQ were equivalent (E/N = 135 Td, $\Delta V_2 = -8.5$ V, and BSQ RF =

426 300 V). Because PIDs are more sensitive to ΔV_2 compared to ΔV_1 we only show the PIDs as a function of ΔV_2 here for

427 simplicity.

429 **3.2 Interlaboratory Comparison of PIDs**

430 We compare PIDs measured from the seven laboratories under lab-defined settings. Acetonitrile and α -pinene were the only
431 VOCs with PIDs measured by every lab. We highlight select VOCs with a particular propensity for water cluster and/or
432 fragment ion formation, that were commonly measured amongst the labs, for a qualitative comparison. We then compare a
433 more diverse suite of VOCs for a quantitative characterization of PIDs across instruments.

434 **3.2.1 Qualitative Comparison of PIDs Across Instruments**

435 Figure 7 highlights differences in PIDs measured from select VOCs common across most of the instruments.

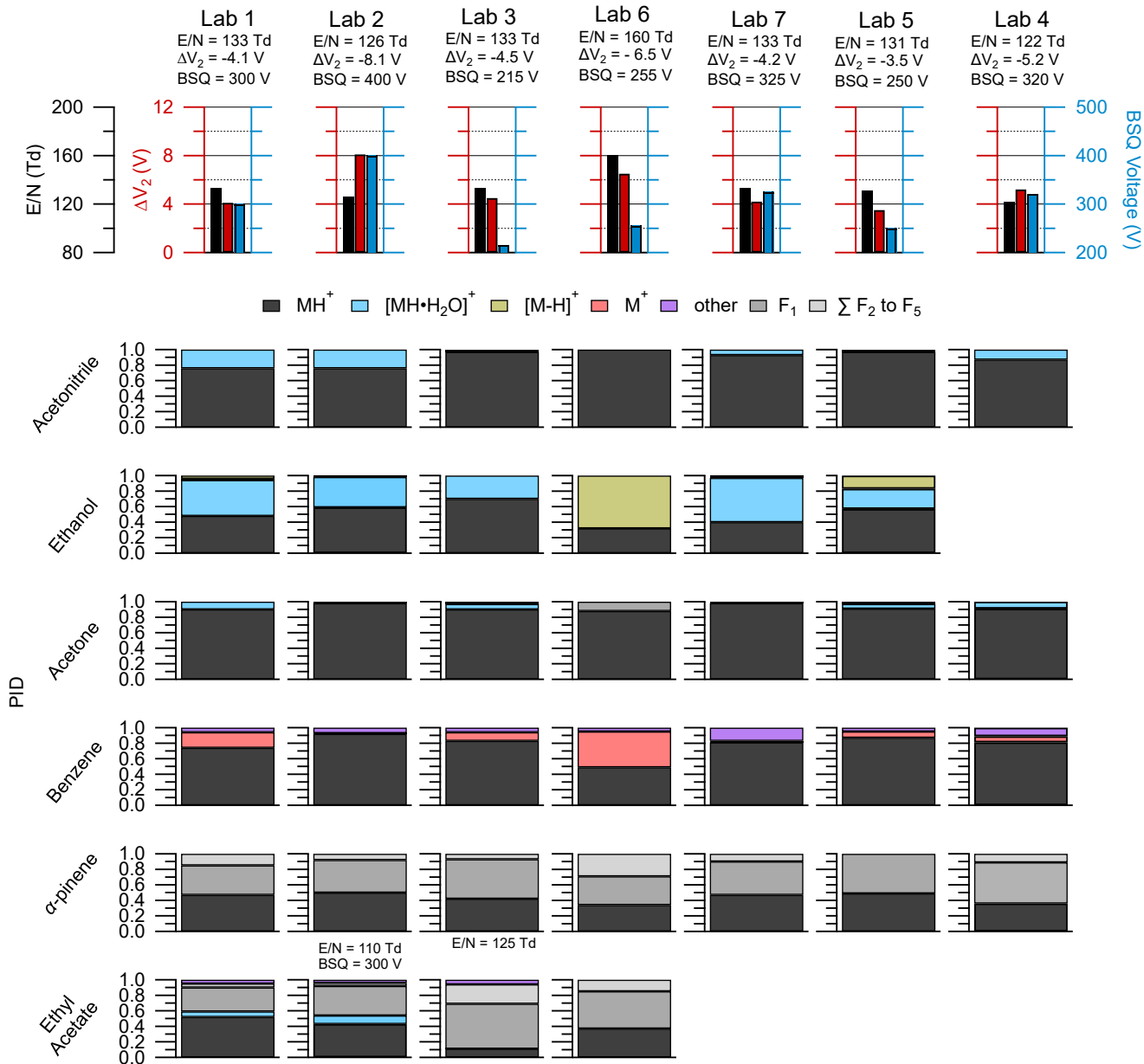


Figure 7: The top row shows the lab identity label (i.e., Lab 1, Lab 2, etc.) and corresponding E/N (left axis, black), ΔV_2 (left axis, red), and BSQ voltages (right axis; blue) used for the PID measurements shown below. PIDs are shown in the lower panels for select VOCs from the interlaboratory comparison dataset and were chosen based on if the VOC measurement was available for each lab. Empty spots where a barplot would be indicate that lab did not have measurements for the VOC in the corresponding row. The PIDs for ethyl acetate were measured for Lab 2 and Lab 3 under slightly different instrumental conditions than the rest of the VOCs and the corresponding E/N and BSQ voltages are shown above the barplots. Contributions of 3 % or less to the PID may be difficult to see in the figure, but exact values can be found in the H_3O^+ PID library.

445 The appearance and contribution of product ions to the PID of a given VOC varied between instruments but can mostly be
446 qualitatively explained by variations in E/N, ΔV_2 , and BSQ voltage. We note that the effects of instrument configuration (i.e.,
447 E/N, BSQ voltage, ion optic voltages) should have predictable effects on PIDs measured by a single instrument and thus using
448 the product ion quantification methods described later in Section 3.5 are not dependent on our ability to reconcile instrument-
449 to-instrument differences.

450
451 Data shown in Fig. 7 originate from instruments operating within a relatively narrow range of E/N (122 Td to 133 Td) with
452 the exceptions of Lab 6 which ran at an E/N of 160 Td and the ethyl acetate measurement from Lab 2. Our analyses of pentanoic
453 acid PID variability as a function of instrument configuration provide some context for interpreting the PID variability observed
454 here. Measurements of the pentanoic acid PID as a function of E/N in Fig. 3 demonstrate that variability in water cluster and
455 fragment product ion contributions to the PID may vary on the order of approximately 10 % when comparing measurements
456 acquired at an E/N of 120 Td versus 130 Td. Similarly, we may expect variability of water cluster contributions for the VOCs
457 shown in Fig. 7 to vary on the order of 10 % within the E/N range of all labs except Lab 6. Water clusters made some
458 contribution to the PID for at least one of the VOCs for each lab except Lab 6 which operated at the highest E/N (160 Td).

459
460 We expected the acetone PID could provide evidence of BSQ low-mass filtering as the m/q of the H^+ adduct ion (m/q 59.05
461 Th) is lower than the water cluster product ion (m/q 77.06 Th) and so lower BSQ voltages may correspond to higher
462 contributions of the H^+ ion to the PID compared to the water cluster. Comparison of the acetone PID from Lab 1 versus Lab 2
463 and Lab 7 displays the opposite trend where, when BSQ voltage increases, the contribution of the H^+ ion increases compared
464 to the water cluster ion. For Lab 2, we suspect this discrepancy in BSQ effect is explained by the mechanism of acetone water
465 clusters formed in the IMR likely declustering after passing through the ΔV_2 ion optic relationship (highest $\Delta V_2 = -8.1$ V
466 indicating potentially important fragmentation/declustering) creating a measured PID entirely consisting of the . However, we
467 do not have an explanation for why Lab 7 does not show water cluster contributions to the acetone PID, where Lab 1 shows
468 about a 10 % contribution, despite having nearly identical settings to the Lab 1 instrument. This comparison of the acetone
469 PID with BSQ voltage demonstrates the challenge of generalizing patterns of PIDs from a single instrument setting to other
470 instruments.

471
472 Each instrument in this intercomparison was operated with a different BSQ voltage which likely influenced variability in PIDs
473 between instruments. For several of the VOCs in Fig. 7 we might expect higher contributions of water clusters to the PIDs for
474 acetonitrile, ethanol, and acetone at higher BSQ voltages because higher voltages decrease the transmission efficiency, relative
475 to water clusters, for the H^+ adduct. For instance, Lab 3 operated with a BSQ voltage of 215 V and Lab 2 operated with a
476 voltage of 400 V representing the lower and upper ends, respectively, of the dataset BSQ voltage range. One possible
477 explanation for the difference in the water cluster contribution to the acetonitrile PID, measured for Lab 3 and Lab 2 of 3 %

478 and 24 % respectively, is increased relative transmission efficiency of the water cluster at the higher BSQ voltage used in Lab
479 2 (both labs have similar E/N).

480
481 Ethyl acetate was also impacted by BSQ voltage effects (Fig. 7). The E/N for the Lab 3 (E/N = 122 Td) measurement of ethyl
482 acetate falls in between that of Lab 1 (E/N = 133 Td) and Lab 2 (E/N = 110 Td) and thus we might expect the PID to be similar
483 to those two labs. In contrast to Labs 1 and 2, the Lab 3 ethyl acetate PID shows a higher contribution of fragment ions and
484 does not show a water cluster contribution. The two major fragment ions for ethyl acetate ($C_2H_3O^+ = 43.02$ Th and $C_2H_5O_2^+ =$
485 61.03 Th) are similar in m/q to the fragment ions of pentanoic acid ($C_3H_5^+ = 41.04$ Th and $C_4H_9^+ = 57.07$ Th) that we saw
486 affected by the BSQ voltage in Fig. 4. Thus, the lower BSQ voltage used for Lab 3 (BSQ = 215 V), compared to Labs 1 (BSQ
487 = 300 V) and 2 (BSQ = 400 V), likely increased the transmission efficiency of fragment ions, relative to the H^+ adduct and
488 water cluster, and increased their contribution to the PID for Lab 3.

489
490 Of the VOCs presented here, α -pinene, shows considerable fragmentation, but also reasonable agreement in the PID (± 10 %
491 for any given product ion contribution to the PID) across instruments. Variability in α -pinene PIDs between instruments can
492 be qualitatively explained by differences in E/N. Lab 6, operating at an E/N of 160 Td (higher fragmentation than the other
493 instruments), showed a near equal contribution of the H^+ adduct, F_1 , and sum of other fragments to the PID whereas the other
494 instruments showed roughly half H^+ adduct, half F_1 , with some (< 10 %) contribution of the sum of other fragments. We expect
495 α -pinene, and most other monoterpenes, to be minimally influenced by changes in BSQ voltage (and thus low-mass filtering
496 effects) as most of the major product ions are greater than m/q 55.04 Th (corresponding to the reagent ion double water cluster,
497 $(H_2O)_2H_3O^+$) where mass-filtering effects are expected to be less pronounced (Krechmer et al., 2018).

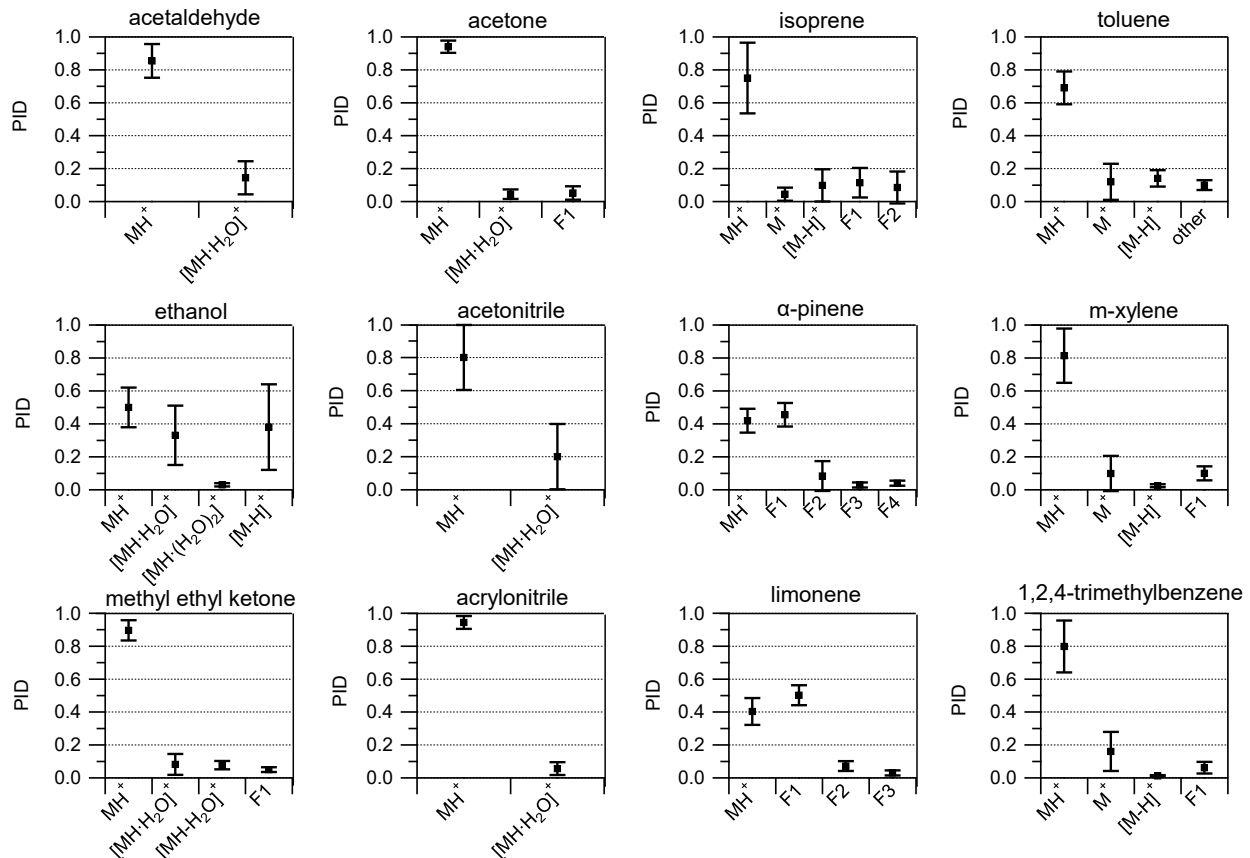
498
499 Reagent ion impurities, O_2^+ and NO^+ , are likely responsible for charge and hydride transfer product ions observed for benzene
500 and ethanol shown in Fig. 7. In Fig. 3 we show that the PID contribution for both hydride (as seen for ethanol and toluene) and
501 charge transfer products (as seen for toluene) increase with increasing E/N. However, variability in E/N does not explain the
502 differences in hydride transfer product contributions to the PID for ethanol and charge transfer product contributions to the
503 PID for benzene between the labs in Fig. 7. Lab 6, which operated with the highest E/N (160 Td), had the largest contributions
504 of both the hydride transfer product for ethanol and the charge transfer product for benzene which is consistent with the
505 observation of more impurity reagent ion chemistry at higher E/N. However, Lab 1 and Lab 7 operated with nearly the same
506 E/N, ΔV_2 , and BSQ voltage, but Lab 7 did not measure the charge transfer product for benzene whereas Lab 1 measured a 20
507 % contribution. We hypothesize that increased inlet flow rates increase O_2^+ and/or NO^+ chemistry as evidenced by the ethanol
508 hydride transfer product making the largest contributions to the ethanol PID for Lab 5 and Lab 6 which operated their
509 instruments at higher flowrates compared to the other labs (Lab 5 = $180\text{ cm}^3\text{ min}^{-1}$ and Lab 6 = $290\text{ cm}^3\text{ min}^{-1}$, while the other
510 systems operated with an inlet flow rate of approximately $100\text{ cm}^3\text{ min}^{-1}$). The increased inlet flowrate may increase mixing
511 of sample air and dilute the water vapor saturated air in the ionization region thus generating more NO^+ and O_2^+ reagent ions.

512

513 We note that several aromatics (e.g., benzene, toluene, chlorobenzene) also generated a product ion, $C_6H_7O^+$, that we could
 514 not identify a mechanism for and we classified as “other”. With regard to benzene detection, this product ion contributed 20
 515 % to the PID for Lab 7 but made smaller contributions (< 5 %) to the PIDs for other labs. In the case of Lab 7, larger
 516 contributions of $C_6H_7O^+$ did not coincide with enhanced contributions of the charge transfer product to the benzene PID so
 517 this ion may not be a product of O_2^+ and/or NO^+ chemistry. Because $C_6H_7O^+$ is generated from several aromatics (see H_3O^+
 518 PID library) it may be an important isobaric interference for phenol.

519 **3.2.2 Quantitative Comparison of PIDs Across Instruments**

520 We calculated the average and standard deviation of the mean of the product ion contributions to the PIDs for 12 VOCs
 521 contained within the interlaboratory comparison dataset (Fig. 8).



522

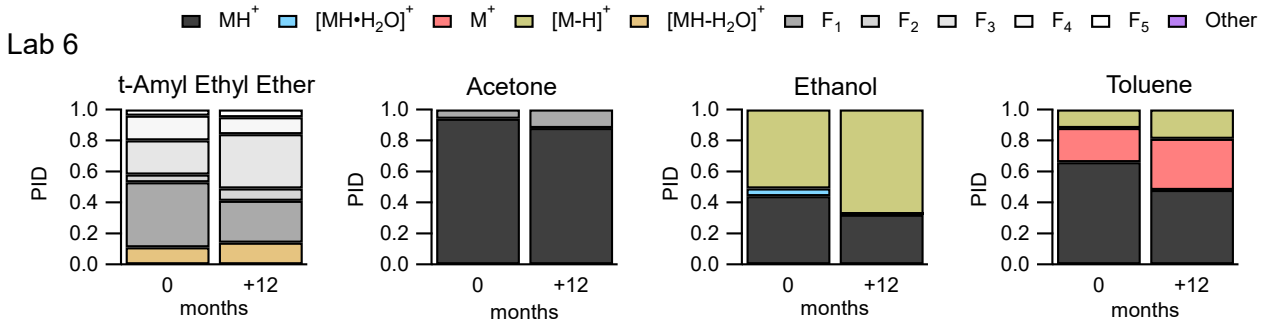
523 **Figure 8: Averages (black squares) and standard deviations of the mean (1 σ) of PIDs for select VOCs. Averages were determined**
 524 **from at least five measurements from the interlaboratory comparison dataset. The number of individual measurements used to**
 525 **calculate average and standard deviation values can be found in Table S1.**

526

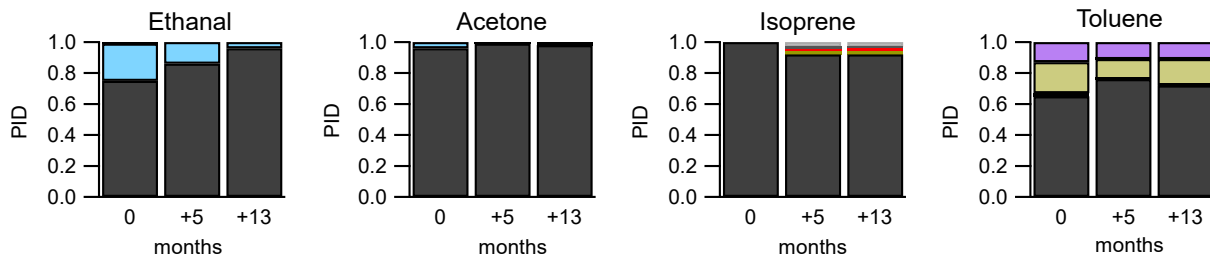
527 In contrast to the reporting uncertainties later discussed in Section 3.6, these averages and standard deviations are meant to
528 quantitatively show variability across the instruments in this study. Many of the VOCs had standard deviations (1σ) for product
529 ion contributions to PIDs that varied by no more than 0.30 thus providing a constraint for predicting PIDs across instruments
530 operating under different conditions. Generally, the relative standard deviation (RSD) of product ion contributions to PIDs
531 was larger for product ions with smaller fractional contributions (e.g., < 0.10) compared to larger contributions (e.g., > 0.30).
532 For instance, the average and standard deviation of the contribution of the MH^+ ion to the methyl ethyl ketone PID was 0.90
533 ± 0.06 (7 % RSD) whereas the water cluster was 0.08 ± 0.06 (75 % relative standard deviation). Ethanol and acetonitrile
534 showed considerable (i.e., > 40 % RSD) product ion variability (Fig. 8). For ethanol, the importance of the water cluster was
535 highly dependent on E/N. Additionally, the fraction of the hydride transfer product ranged from < 0.05 to roughly 0.50. The
536 ethanol and acetonitrile PIDs are not only influenced by E/N but also likely impacted by the BSQ voltage since the H^+ adducts
537 are a relatively low m/q (i.e. m/q < 55.04 Th). VOCs like isoprene and the aromatics have PIDs that are impacted by NO^+ and
538 O_2^+ reagent ion chemistry which, as discussed above, is difficult to predict without directly measuring PIDs of susceptible
539 VOCs. The general trend of fragmentation/declustering with increasing E/N and ΔV_2 can be used as a guideline to inform a
540 user how they might expect their PIDs to deviate from the averages shown in Fig. 8. We recommend the H_3O^+ PID library as
541 guide for estimating PIDs for VOCs measured with Vocus PTR-ToF-MS instruments in the absence of direct measurements.

542 **3.2.3 Consistency of PIDs Measured Over Time**

543 Two labs, Lab 6 and Lab 7, provided data where the instrument was operated under the same voltage configurations, but PIDs
544 were measured a year or more apart. Figure 9 shows the variability in PIDs for four select VOCs from these two labs over a
545 year.



Lab 7



546

547 **Figure 9: PIDs for select VOCs from Lab 6 (top frames) and Lab 7 (bottom frames) showing variability of PIDs over one year.**

548

549 Measurements from both labs indicate that, given the same voltage configurations on the same instrument, PIDs can change
 550 over time. The largest change from the subset of VOCs in Fig. 9 is the water cluster contribution to the ethanal (acetaldehyde)
 551 PID, from Lab 7, starting at 24 % and decreasing to 4 % after 13 months. Isoprene from Lab 7 has fragment and charge/hydride
 552 transfer product ions that appear in the PID after five months.

553

554 The PIDs for the four VOCs from Lab 6 show greater contributions of fragment and charge/hydride transfer product ions after
 555 12 months compared to the first measurement. We hypothesize three possible factors could be related specifically to the
 556 increase in charge/hydride transfer product ions over time: (1) the increase in inlet flowrate ($260 \text{ cm}^3 \text{ min}^{-1}$ at 0 months to 290
 557 $\text{cm}^3 \text{ min}^{-1}$ at +12 months), (2) capillary insertion depth, and (3) leaks into the sampling system from maintenance. Lab 6 reports
 558 that after maintenance on their instrument changes in instrument performance (e.g., sensitivity) were observed and may be
 559 associated with cleaning the capillary that serves as the inlet to the instrument (Jensen et al., 2023). The instrument was in a
 560 stable condition after maintenance before the PIDs were collected. Although we did not observe a strong dependence of NO^+
 561 and O_2^+ chemistry on capillary insertion distance for the Lab 1 instrument (Fig. S5), it is possible that at the higher inlet
 562 flowrates, used for the Lab 6 measurements, an effect could be observed.

563

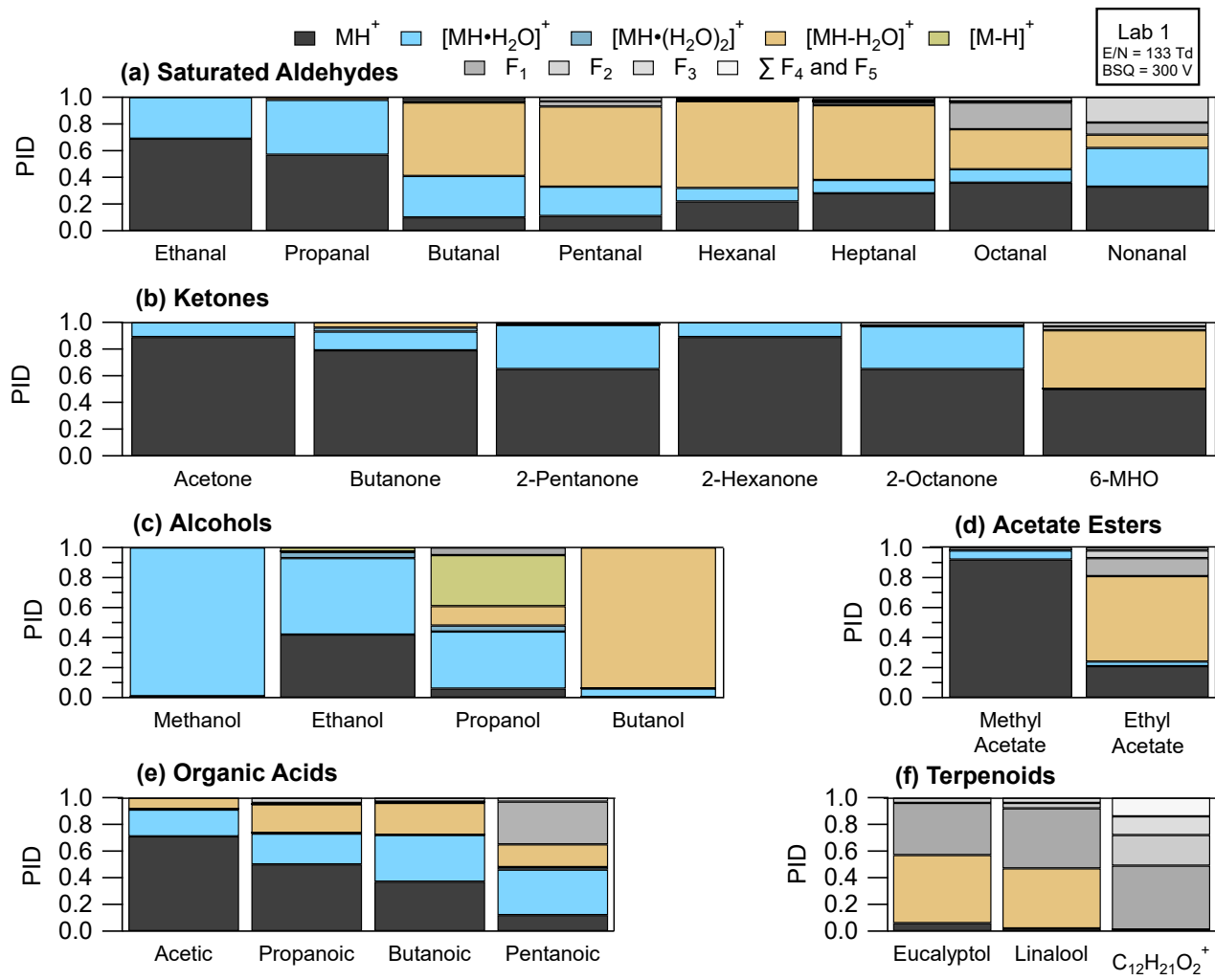
564 None of the product ions from this example change their contribution to the PID by more than 10 % over time—with the
 565 exception of the ethanal water cluster. This time-dependent variability in PIDs demonstrated in Fig. 9 points to some factor or

566 combination of factors affecting PIDs not considered in our analyses (e.g., degradation of the microchannel plate detector
567 (Müller et al., 2014) or possibly ion source degradation). Additionally, the variability of individual product ions over time
568 provides an estimate of aging variability on the order of 10 % (but as high as 20 %).

569 **3.3 Measurements of PIDs for Oxygenated VOCs from Lab 1**

570 We highlight features of PID formation from VOCs with oxygenated functionalities that may be measured in high
571 concentrations from samples of indoor air and/or urban air plumes in the sections below. Product ion formation is characterized
572 in the literature for some VOCs like aromatics and monoterpenes (Yuan et al., 2017; Misztal et al., 2012; Materić et al., 2017;
573 Kari et al., 2018) that do not readily form water clusters. Product ion formation from oxygenated VOCs is less well-
574 characterized, particularly for water cluster formation.

575
576 Figure 10 shows PIDs for select VOCs categorized by functional group as measured from Lab 1 using calibration standards
577 (except for the unidentified monoterpene acetate ester which was measured from a restroom air sample). PIDs were measured
578 under instrument settings that correspond to Lab 1b in Table 1. A key result demonstrated in Fig. 10 is that, for the subset of
579 VOCs shown here, the H^+ adduct contribution to the PID is often less than 60 % and thus air samples containing these VOCs
580 may have many product ions populating the mass spectra. In other words, H_3O^+ ionization (including NO^+ and O_2^+ impurities)
581 is generating unintended product ions often at similar rates as the intended H^+ adduct for most VOCs. Below we discuss general
582 patterns of product ion formation from VOCs with varying functionalities.



583
584 **Figure 10: PIDs measured for Lab 1 for select VOCs representing different functional groups. VOCs from left to right, per functional**
585 **group, are in order of increasing carbon number. “ $\text{C}_{12}\text{H}_{21}\text{O}_2^+$ ” is an unidentified monoterpene acetate ester, measured from a**
586 **restroom air sample, likely originating from isobornyl or linalyl acetate (Link et al., 2024).**

587 3.3.1 Saturated Aldehydes

588 Recently, fragment product ions from saturated aldehydes have been highlighted in measurements of urban air influenced by
589 cooking emissions (Coggon et al., 2024), ozonolysis of sea water (Kilgour et al., 2024), and ozonolysis products of human
590 skin oils in indoor air (Wang et al., 2024; Ernle et al., 2023). In the Lab 1 instrument fragment product ions contributed > 40
591 % to the PID for saturated aldehydes with a carbon number greater than three (i.e., butanal to nonanal). Water cluster formation
592 contributed > 20 % to the PID for ethanal (acetaldehyde), propanal, and nonanal. As reported previously for butanal through
593 heptanal (Buhr et al., 2002), the fragment ion making the largest contribution to the PID in the Lab 1 instrument was the

dehydration product (i.e., $[\text{MH}-\text{H}_2\text{O}]^+$). We find additional agreement with previous literature reporting octanal and nonanal fragmentation to smaller product ions (e.g., C_5H_9^+ , C_3H_5^+ , $\text{C}_6\text{H}_{11}^+$). We suspect, from limited experimental data (ŠPaněl et al., 2002), that larger saturated aldehydes (e.g., decanal) may also produce fragment product ions smaller than the dehydration product ion in the Lab 1 instrument. However, as the carbon number of the saturated aldehyde increases, from butanal, the contribution of the H^+ adduct to the PID increases—and the contribution of dehydration and fragment product ions decrease—suggesting larger aldehydes fragment less overall than butanal, pentanal, and hexanal. Finally, we note we cannot easily explain the formation of some product ions from H_3O^+ ionization from typical mechanisms (e.g., C_5H_9^+ from nonanal) and thus we hypothesize that reactions involving NO^+ and/or O_2^+ may be responsible for the generation of some fragment ions from saturated aldehydes.

3.3.2 Ketones

In contrast to saturated aldehydes, and consistent with previous work (Buhr et al., 2002), the saturated ketones (i.e., all the ketones in Fig. 10b except 6-MHO) measured with the Lab 1 instrument do not fragment substantially (i.e., sum of fragment contributions to PID < 5 %). However, the saturated ketones do form water clusters with contributions ranging from 10 % (e.g., acetone) to 40 % (e.g., 2-octanone) to the PID. We do not observe a clear relationship between increasing carbon number and water clustering. In fact, when comparing 6-methyl-5-hepten-2-one (6-MHO) and 2-octanone, two eight carbon molecules, the water cluster for 2-octanone contributed 40 % to the PID whereas 6-MHO had no detectable water cluster formation (Fig. 10b). Additionally, as demonstrated by the PID from 6-MHO, adding carbon branching and/or additional functionalities can change product ion formation considerably compared to 2-octanone—the saturated C_8 ketone analogue.

3.3.3 Alcohols

We observed important contributions of water clusters (> 40 %) to the PIDs measured for methanol, ethanol, and propanol. Methanol and ethanol can be present in concentrations that exceed 1 nmol mol^{-1} in both outdoor and indoor air (Nazaroff and Weschler, 2024) and thus the water clusters of these two alcohols may make important contributions to sample mass spectra. We also measured small contributions of double water clusters to the PID from ethanol and 2-propanol (4 % for each VOC). Previous studies have shown considerable fragment product ion production from dehydration of alcohols (Buhr et al., 2002; ŠPaněl et al., 2002; Warneke et al., 2003; Pagonis et al., 2019) and we also observed that for 2-propanol and 1-butanol. For 1-butanol > 90 % of the PID was from the dehydration product ion and we did not measure any generation of the H^+ adduct. We also observe small contributions of the hydride transfer product from ethanol that have been reported from another PTR-ToF-MS (Coggon et al., 2024) and measured with the NO^+ reagent from a selected ion flow tube study (ŠPaněl et al., 2002). The hydride transfer product made a 30 % contribution to the PID measured for 2-propanol. As summarized in Koss et al. (2016), several other saturated alcohols have hydride transfer enthalpies that decrease with increasing carbon number and thus hydride transfer product ions may appear in PTR-MS spectra from ambient air samples where saturated alcohols may be in high

625 abundance. As an example, Buhr, et al. (2002) measured 10 % contribution of the hydride transfer product from 1-octanol and
626 2-octanol to their PIDs.

627
628 Although we focus on reaction with NO^+ as the primary reagent producing hydride transfer products from reaction with VOCs,
629 Hegen et al. (2023) hypothesized that charge transfer from O_2^+ to methanol, with subsequent loss of hydrogen atom, may be
630 an important mechanism for creating product ions that appear in the mass spectrum as hydride transfer products. Thus, both
631 charge and hydride transfer enthalpies may be useful qualitative indicators for predicting if $[\text{M}-\text{H}]^+$ product ions are generated
632 from ionization of alcohols. For VOCs whose PIDs are not included in the H_3O^+ PID library, we refer the reader to Koss et al.
633 (2016) for a table of hydride and charge transfer enthalpies for many VOCs measured using PTR-MS as a useful resource for
634 predicting the possible generation of product ions.

635 **3.3.4 Acetate Esters, Organic Acids, and Oxygenated Monoterpenes**

636 Neither the acetate esters nor oxygenated monoterpenes in this study show a propensity to form water clusters. We measure
637 considerable fragmentation of ethyl acetate (Fig. 10d). In addition to ethyl acetate, Buhr et al. (2002) measured major
638 contributions of fragmentation products of several other acetate esters to their PIDs. Although Buhr et al. (2002) used an older
639 model of PTR-MS with a drift tube ionization region, we expect that larger acetate esters may also fragment to the same degree
640 as observed in that study in the Vocus PTR-ToF-MS.

641
642 Alkanoic acids have PIDs that show complexity similar to the saturated aldehydes with extensive water cluster formation and
643 fragmentation (Fig. 10e). Notably, the fraction of H^+ adduct in the PID decreases with increasing carbon number with roughly
644 15 % of the PID for pentanoic acid allocated to the H^+ adduct. More data is needed, but this trend suggests larger organic acids
645 (i.e., $> \text{C}_5$) may also produce water cluster and fragment product ions in similar abundance to the H^+ adduct. Characterization
646 of PIDs for larger (e.g., C_9 and C_{10}) acids may be of particular importance for measurements of early generation oxidation
647 products of terpenes.

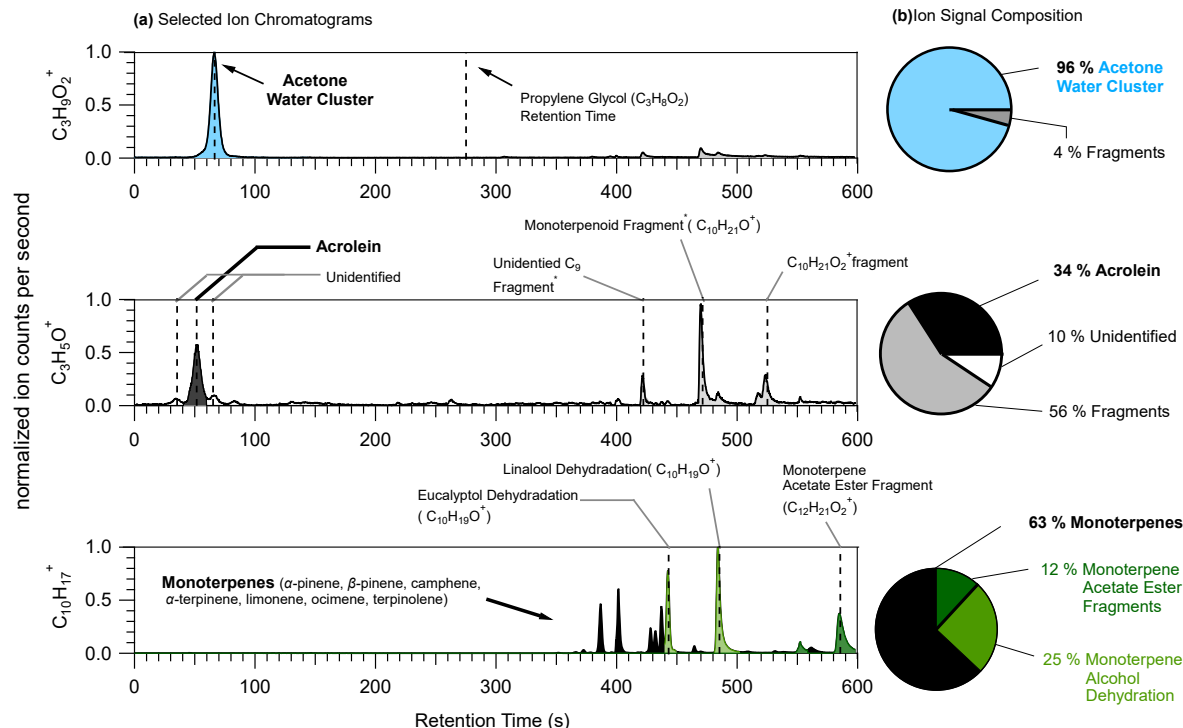
648
649 Notably, the contribution of the H^+ adduct to the PID for the terpenoids highlighted here are all less than 5 %. The monoterpene
650 alcohols (eucalyptol and linalool) generate dehydration product ions with abundances greater than 40 % (Fig. 10f). The
651 dehydration product of the monoterpene alcohols, $\text{C}_{10}\text{H}_{17}^+$, is isobaric (i.e., occurring at the same m/q) with the H^+ adduct for
652 monoterpenes. We also highlight the PID measured for $\text{C}_{12}\text{H}_{21}\text{O}_2^+$, a monoterpene acetate ester (most likely linalyl or isobornyl
653 acetate based on offline GC analysis presented in Link, et al. (2024)), measured from a restroom air sample. This ion fragments,
654 losing a neutral acetic acid, to form $\text{C}_{10}\text{H}_{17}^+$ suggesting monoterpene acetate esters may also create monoterpene interferences
655 from samples where monoterpenes and the acetate esters are both present.

656 **3.4 Mass Spectral Ambiguity from the Influence of PIDs: A Restroom Air Sample Case Study**

657 One consequence of multi-product ion generation in PTR-MS is that if PIDs are unknown or uncharacterized they can create
 658 ambiguity when identifying peaks in the mass spectrum in the absence of a pre-separation method. In particular, studies
 659 performing non-targeted analysis of the ion signals measured by PTR-MS from indoor air samples (Link et al., 2024; Ditto et
 660 al., 2023; Mattila et al., 2021; Liu et al., 2024; Klein et al., 2016) may be challenged by the presence of unintended product
 661 ions generated by high concentrations of parent VOCs. For instance, Ernle et al. (2023) recently demonstrated the challenge
 662 of quantifying isoprene from m/q 69.07 ($C_5H_9^+$) because of interferences from fragments of aldehydes generated from ozone
 663 skin oil oxidation indoors. We briefly demonstrate several challenges related to product ion generation and resulting mass
 664 spectral ambiguity using a measurement of ambient air in a restroom as a case study.

665

666 High concentrations of terpenoids emitted from fragrant urinal screens reacted with ozone to create oxidized VOCs in the
 667 restroom we sampled from. Fig. 11 shows the selected ion chromatograms for three ions measured, using GC-PTR-ToF-MS,
 668 from the restroom air sample to demonstrate challenges associated with product ion formation.



669

670 **Figure 11:** (a) Selected ion chromatograms (left) of three ions for which PIDs present challenges: $C_3H_9O_2^+$ (top), $C_3H_5O^+$ (middle),
 671 and $C_{10}H_{17}^+$ (bottom). Dotted vertical lines are placed at the retention times assigned to VOCs or parent ion species either directly
 672 measured from calibration sources or supported by time series correlations with known product ions. Peak assignments with an
 673 asterisk are species that were assigned from product ion time series analyses. (b) Pie charts showing the ion signal composition with
 674 contributions from the VOC typically assigned to the ion (black) and contributions from interfering product ions. Product ion

675 contributions to the ion signal are determined by integrating areas of all the major peaks, calculating the relative contribution of
676 each peak to the total area of all the identified peaks, and classifying them by product ion identity.
677

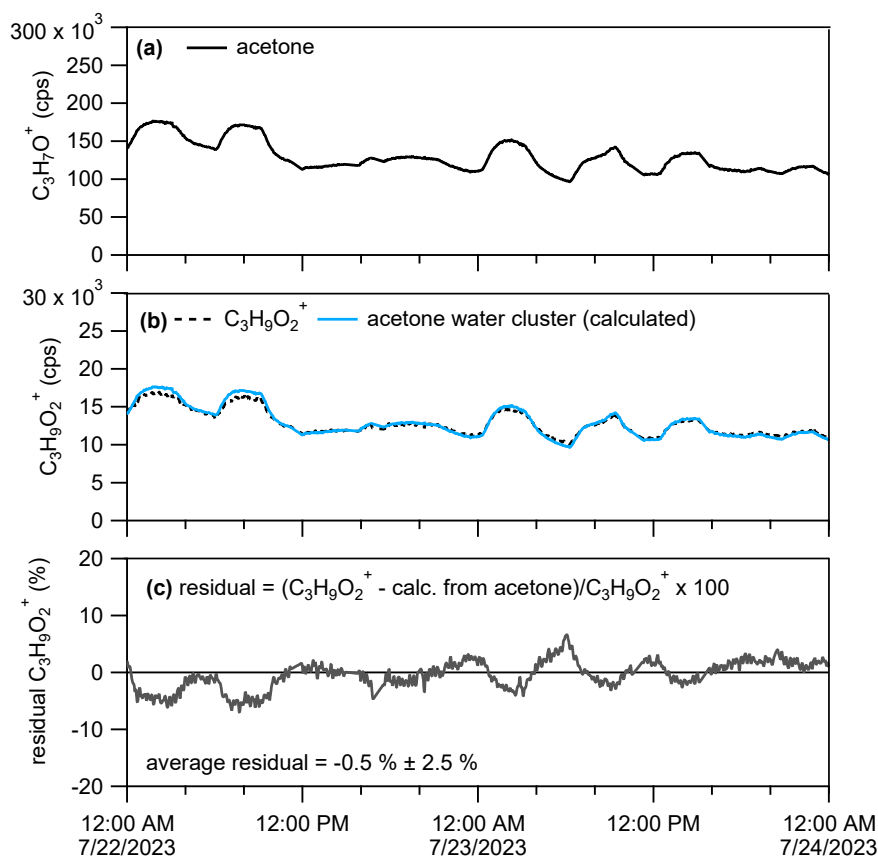
678 In the restroom the ion possibly attributable to propylene glycol, $C_3H_9O_2^+$ (Hopstock et al., 2024), was found to be mostly
679 comprised of the acetone water cluster. Acetone generates a water cluster with a roughly 10 % efficiency in the Lab 1
680 instrument used for this restroom measurement. Acetone concentrations are generally elevated indoors, compared to outdoors,
681 and in the restroom acetone concentrations were elevated at approximately 20 nmol mol⁻¹ (equivalent to 20 parts-per-billion).
682 Recent studies have used PTR-MS for the measurement of VOCs, including propylene glycol, in the smoke of electronic
683 cigarettes (Bielik et al., 2024; Hopstock et al., 2024; Sheu et al., 2020). Sheu et al. (2020) could not quantify possible
684 contributions of propylene glycol to thirdhand smoke indoors because of the acetone water cluster interference. This $C_3H_9O_2^+$
685 interference from acetone water cluster may be most pronounced indoors where air can contain elevated acetone concentrations
686 from human breath and materials emissions (Molinier et al., 2024).

687
688 Acrolein (C_3H_4O) is a hazardous indoor air pollutant (Seaman et al., 2007; Logue et al., 2011) and recently was measured,
689 using PTR-MS, from a residential test facility (Arata et al., 2021) where concentrations were high enough such that it was the
690 largest source of gas-phase hazardous exposure (Hodshire et al., 2022). In the restroom the $C_3H_5O^+$ ion signal (i.e., the H^+
691 adduct ion commonly attributed to acrolein) experienced considerable interferences from fragmentation of VOCs containing
692 nine (C_9) to twelve (C_{12}) carbon atoms. There were some additional interferences from unidentified sources—one of which
693 may be the propanal hydride transfer product (could not confirm here due to coelution of acetone). In the restroom where
694 terpenoid (monoterpene, monoterpene alcohols, and monoterpene acetate esters) concentrations were roughly 20 nmol mol⁻¹
695 the fragmentation of two ions likely attributable to terpenoids, $C_{10}H_{21}O^+$ and $C_{10}H_{21}O_2^+$, make important contributions (56 %)
696 to the $C_3H_5O^+$ ion signal. We note that the terpenoids emitted from the urinal screens created high concentrations that may
697 uniquely impact the $C_3H_5O^+$ signal compared to other indoor environments. However, this observation points to the possible
698 unexpected impact of consumer product emissions on indoor air measurements of acrolein.
699

700 We highlight here the possible interferences on the $C_{10}H_{17}^+$ ion, normally attributed to monoterpene isomers, from
701 fragmentation reactions of monoterpene alcohols (eucalyptol and linalool) and monoterpene acetate esters (likely isoborynl or
702 linalyl acetate). Previous studies have pointed to $C_{10}H_{17}^+$ interferences from dehydration of monoterpene alcohols of biogenic
703 origin (Joó et al., 2010; Kari et al., 2018; Demarcke et al., 2010). In the restroom we found 25 % of the $C_{10}H_{17}^+$ signal was
704 attributable to dehydration of linalool and eucalyptol which were emitted from urinal screens. This highlights how in indoor
705 spaces personal care products and scented consumer goods can emit terpenoids (not typically measured in high concentrations
706 from biogenic sources) in high concentrations that can complicate the measurement of monoterpene using PTR-MS without
707 pre-separation. Additionally, we show a $C_{10}H_{17}^+$ interference from loss of acetic acid from monoterpene acetate esters which
708 is possibly a problem unique to the measurement of indoor air.
709

710 **3.5 Using PIDs to Improve Identification and Quantification of VOCs from PTR-MS Measurements**711 **3.5.1 Method 1: Estimating Product Ion Abundance from Real-Time Data**

712 In Section 3.4 we demonstrated the interference of acetone water cluster on the ion signal, $C_3H_9O_2^+$, that might be typically
713 attributed to propylene glycol (Fig. 11) using a chromatographic pre-separation. If a PID has been measured from a calibration
714 source, it can be used to estimate the abundance of product ions to an ion signal relative to another ion from real-time data.
715 For example, we can determine the influence of acetone water cluster on the $C_3H_9O_2^+$ ion signal measured by the PTR-MS,
716 without chromatographic pre-separation (“real-time data”), by calculating the expected contribution predicted by the acetone
717 PID. We show an example of how we estimated the influence of acetone water cluster on the real-time $C_3H_9O_2^+$ ion signal in
718 Figure 12.



719
720 **Figure 12: (a) Time series for $C_3H_7O^+$ attributable to acetone. (b) Time series for $C_3H_9O_2^+$ with the raw signal (black**
721 **dotted line) and $C_3H_9O_2^+$ calculated to be attributable to acetone water cluster (10 % contribution to acetone PID).** (c)

722 **Percent residual $C_3H_9O_2^+$ ion signal after subtracting out the estimated contribution from acetone water cluster.**

723

724 We measured the PID for acetone (as shown in Fig. 10 and listed in the H_3O^+ PID library) as 0.90 H^+ adduct ($\text{C}_3\text{H}_7\text{O}^+$) and
725 0.10 water cluster ($\text{C}_3\text{H}_9\text{O}_2^+$). Assuming contributions of isomers or product ions to the $\text{C}_3\text{H}_7\text{O}^+$ signal are negligible, we can
726 divide the product ion fraction for $\text{C}_3\text{H}_9\text{O}_2^+$ ($f_{[\text{MH}\cdot\text{H}_2\text{O}]^+}$) by the product ion fraction for $\text{C}_3\text{H}_7\text{O}^+$ (f_{MH^+}) to get the fraction of
727 acetone water cluster relative to acetone H^+ adduct ($\frac{f_{[\text{MH}\cdot\text{H}_2\text{O}]^+}}{f_{\text{MH}^+}}$). We can then multiply this fraction by the $\text{C}_3\text{H}_7\text{O}^+$ signal (S_{MH^+})
728 to get the contribution of acetone water cluster to the $\text{C}_3\text{H}_9\text{O}_2^+$ signal ($S_{[\text{MH}\cdot\text{H}_2\text{O}]^+}$) following Equation 2,

$$729 S_{[\text{MH}\cdot\text{H}_2\text{O}]^+} = S_{\text{MH}^+} \cdot \frac{f_{[\text{MH}\cdot\text{H}_2\text{O}]^+}}{f_{\text{MH}^+}} \quad (2)$$

730 Multiplying the $\text{C}_3\text{H}_7\text{O}^+$ signal (shown in Fig. 12a) by $\frac{f_{[\text{MH}\cdot\text{H}_2\text{O}]^+}}{f_{\text{MH}^+}}$ (i.e., $0.10/0.90 \approx 0.11$) generates an estimated $\text{C}_3\text{H}_9\text{O}_2^+$ ion
731 signal time series (Fig. 12b, blue trace) that is from the acetone water cluster. In Fig. 12c we calculate the percent residual
732 $\text{C}_3\text{H}_9\text{O}_2^+$ signal, after subtracting out the estimated contribution of acetone water cluster. The average residual of -0.5 %
733 indicates that nearly all of the $\text{C}_3\text{H}_9\text{O}_2^+$ ion signal measured from the restroom is from acetone water cluster which is consistent
734 with what we measured from the chromatographic separation in Fig. 11a. Although not shown in this example of $\text{C}_3\text{H}_9\text{O}_2^+$, if
735 after applying this method residual signal remained, and was consistently above zero, that could indicate ion signal related to
736 H^+ adducts of VOCs or influences of other product ions. We verified that the $\text{C}_3\text{H}_7\text{O}^+$ signal we measured from the restroom
737 (using GC) was > 95 % (with some possible contribution from propanal and contributions of fragment ions) attributable to
738 acetone thus suggesting that application of this method may work best when supplemented with a GC measurement.

739 We point to the study of Coggon et al. (2024) for further demonstrations of how to separate the influence of product ions on
740 H^+ adduct ions for benzene (C_6H_7^+), isoprene (C_5H_9^+), and ethanal (acetaldehyde, $\text{C}_2\text{H}_5\text{O}^+$) measured from outdoor air
741 influenced by oil and gas and cooking emissions. When directly measuring PIDs using a calibration source is not possible, the
742 H_3O^+ PID library included with this manuscript can serve as a useful source for estimating possible product ion interferences.
743 The existing PTR library compiled by Pagonis et al. (2019) contains measurements of fragment product ions that can also
744 provide product ion data relevant for instruments other than the Vocus. This product ion estimation method may produce
745 reasonable results for some VOCs like acetone, but many ions will often have multiple isomers or isobaric product ion
746 interferences that challenge accurate application of the method.

748 3.5.2 Method 2: Using Product Ions for Quantification

749 PTR-MS quantification is often performed using calibrations of an H^+ adduct signal for a target VOC (e.g., $\text{C}_3\text{H}_7\text{O}^+$ for
750 acetone), but the PTR-MS can also be calibrated to product ions. Coggon et al. (2024) showed that benzene concentrations
751 calculated from the charge transfer product ion (C_6H_6^+) calibration agreed with concentrations quantified from GC
752 measurements. The authors concluded that the benzene charge transfer product ion (C_6H_6^+), which had no interferences, was
753 a more suitable signal to quantify benzene from than the H^+ adduct (C_6H_7^+), which suffered interferences from fragmented

754 aromatics. However, pre-separation was used in that study to verify the charge transfer product was free of interferences. In
755 principle, any product ion that is free of interferences could be used as an alternative to the H⁺ adduct for quantification.

756 **3.5.3 Method 3: Supplemental Measurement with a GC**

757 It is worth acknowledging the value of a supplemental measurement using GC. When directly interfaced to the PTR-MS, GC
758 can be used to measure PIDs and aid in identifying ion signals from the real-time PTR-MS measurement. Benchtop GCs
759 optimized for thermal desorption measurements can also be used in offline analysis to identify possible sources of ion
760 interferences. Although not discussed here, isomers are confounding influences on the interpretation of ion identities and GC
761 is also useful for quantification of VOC isomers. Nevertheless, not all VOCs present in an air sample are likely to be
762 independently separated (e.g., sesquiterpenes for mid-polarity columns) or trapped and desorbed via a preconcentration system.

763 **3.6 The H₃O⁺ PTR PID Library and Recommendations for Reporting Product Ion Uncertainty**

764 We have compiled the data presented in this manuscript into a library included in the supplement. The library will be updated
765 as new observations are included and the updated library can be found online (NIST, 2024). The measurements included in
766 the library were collected under different instrument conditions (listed under the “2_Lab_ID” tab of the library spreadsheet)
767 so care should be taken to most closely compare PIDs reported in this library to PIDs collected on an instrument with a similar
768 configuration (i.e., similar E/N, BSQ voltage, ion optic voltages, flowrates). There is an inherent precision with which PIDs
769 can be measured following the GC-based method we have demonstrated. To constrain the uncertainty associated with the PIDs
770 in the H₃O⁺ PTR PID Library, we evaluate the variability in PIDs determined from a single measurement of a VOC (Fig. S6)
771 and the variability observed in PIDs measured from select VOCs over three weekends from restroom air samples compared to
772 the PID library measurement performed six months earlier (Fig. S7).

773

774 We observe that for a single measurement, the contribution of a given product ion to the PID for nonanal varies by no more
775 than 0.01 fractional units (Table S2). For repeat measurements over time (three weeks for the restroom examples shown here),
776 we observe that the absolute variability in product ion contributions to a PID is largest for product ions with the largest relative
777 contributions to the PID (Table S3). For example, from the restroom samples, the fractional contribution of C₇H₉⁺ to the toluene
778 PID ranged from 0.71 to 0.78 (a 0.07 fractional unit range) over the three weekends whereas the contribution of C₆H₇O⁺ ranged
779 from 0.04 to 0.06 (a 0.02 fractional unit range). For both single measurements and the repeat PID measurement example shown
780 in Fig. S7, the relative standard deviation of calculated fractional product ion contributions increases as the absolute
781 contribution decreases.

782

783 Thus, we define uncertainty to ranges of product ion fractional contributions to a PID, for a single measurement and repeat
784 measurements performed on the timescale of weeks, as shown in Table 3.

785 **Table 3: Observed and Recommended Uncertainties for Ranges of Product Ion Contributions to a PID for VOCs in**
 786 **the PTR H₃O⁺ Library.**

Product Ion Fractional Contribution to PID Range	Single Measurement Uncertainty	Repeat Measurement Uncertainty	Recommended Reporting Uncertainty
> 0.30	5 %	6 %	15 %
0.16 to 0.30	5 %	10 %	20 %
0.04 to 0.15	11 %	30 %	30 %
< 0.04	50 %	100 %	100 %

787 The "single measurement uncertainty" reflects the precision with which the fractional contribution of a given product ion to a
 788 PID can be determined from a single measurement. We derived the ranges shown in Table 3 from the calculation of the nonanal
 789 PID from a GC measurement. We assume this uncertainty is not chemical dependent and thus applies to other chemicals. The
 790 "single measurement uncertainty" values are a conservative estimate of the uncertainty associated with the calculation of a
 791 product ion contribution to a PID when measured using the GC method.

792 The "repeat measurement uncertainty" reflects the precision of a product ions fractional contribution to a PID when repeatedly
 793 measured over the timescale of weeks (supported by the measurements from the restroom shown in Fig. S7). We used the
 794 variability in product ion contributions calculated for the acetic acid, acetone, and toluene PIDs shown in Fig. S7 and in Table
 795 S3 to constrain the "repeat measurement uncertainty". We find that the relative standard deviation from repeat measurements
 796 of product ion contributions over three weeks is greater than that of a single measurement (Table 3).

797 We derive a recommended reporting uncertainty by comparing the average and standard deviations of the product ion
 798 contributions to the PIDs for acetic acid, acetone, and toluene—measured in the restroom samples—to their corresponding
 799 entries in the H₃O⁺ PTR-MS PID Library. The PID measurements presented in the library (for Lab 1b) were acquired
 800 approximately six months prior to the restroom measurements. Thus, the recommended reporting uncertainty provided in Table
 801 3 incorporates our constraints on "repeated measurement uncertainty" as well as an estimate of the stochastic variability in
 802 PID development that can occur over months as is demonstrated earlier in Fig. 9. By applying the recommended reporting

803 uncertainties to the average product ion contributions measured for the PIDs of the three VOCs in the restroom samples, we
804 find that the average restroom values come into range of the values in the PID library (Table S3).

805 **3.7 Recommendations for Mitigating Challenges from Unintended Product Ion Generation**

806 As demonstrated in the interlaboratory comparison data, PTR-MS users are likely to experience unintended product ion
807 generation under a variety of instrument operating conditions. We recommend several practices that PTR-MS users can adopt
808 to improve the interpretability of PTR-MS data:

- 809 ▪ Measure PIDs regularly: Surrogate analytes can be used (and included in calibration source cylinders) to provide
810 some indication of how likely it is a mass spectrum may be influenced by certain types of product ions. For example,
811 benzene can be used as a surrogate for charge transfer reaction chemistry, acrolein (data shown in the H_3O^+ PTR PID
812 Library) for water clustering, and α -pinene for fragmentation. Because PIDs can change over time, regularly (at least
813 once a month during periods of active measurements) measuring the PIDs of a few key surrogates can provide relative
814 information on how the PIDs of other VOCs may also be changing. The ion chemistry presented in Table 1 can act
815 as a guide for users to evaluate if ions appearing in a mass spectrum could be generated from unintended product
816 ions. Additionally, the step-by-step procedure outlined in the Supplement can serve as a method for measuring PIDs.
- 817 ▪ Optimize analyte detection with instrument tuning: Here we demonstrated IMR E/N and BSQ voltage affected PIDs.
818 A user can measure the PID of target analytes and scan E/N and BSQ voltage values to optimize the production of a
819 desired product ion (e.g., the H^+ adduct). Because cluster and fragmentation product ions are generated and detected
820 more efficiently at different extremes of E/N and BSQ voltage values instrument tuning will not eliminate unintended
821 product ion generation.
- 822 ▪ Refer to the H_3O^+ PTR PID Library: For the VOCs available in the library (NIST, 2024) a user can identify
823 problematic m/q and elemental formula associated with unintended product ions from VOCs known to be in a sample
824 (including multi-component calibration sources).
- 825 ▪ Measure the instrument sample flowrate regularly: We provide evidence suggesting an influence of flowrate on PIDs,
826 but we also note that the sample flowrate will also affect instrument sensitivity (Jensen et al., 2023). When sampling
827 from pristine environments measuring the sample flow once a week may be sufficient. For measurements of urban or
828 indoor air measuring the flow once a day is recommended. Higher frequency flow checks may be necessary for
829 measurements where particulate matter loading is high (e.g., fire research laboratory burn samples, cooking
830 emissions, etc.).
- 831 ▪ If possible, use a supplemental measurement, GC or otherwise, to support identification of ions measured with PTR-
832 MS from multi-component air samples.
- 833 ▪ Define the acceptable level of accuracy for your measurement: PTR-MS provides high time resolution measurements
834 of VOCs in air that cannot be achieved with many techniques. For non-targeted analyses, identifying and accounting
835 for all influences of unintended product ions is currently impractical. Studies that seek to quantify all VOCs measured,

836 both known and unknown, by the PTR-MS may suffer from greater uncertainties arising from unintended product ion
837 generation. While more uncertain, these non-targeted analyses are important for progressing research. On the other
838 hand, users seeking to quantify specific VOCs (e.g., air toxics or hazardous air pollutants) for the purposes of
839 measurements supporting regulations will need to account for product ion chemistry for high accuracy measurements.

840 **4 Summary and Conclusions**

841 Here we outlined general rules for identifying possible product ion interferences based on common reaction mechanisms that
842 can occur when using PTR-MS. Additionally, the method of product ion classification (using ion formula predicted from
843 mechanisms) used here can be employed in future studies to continue to develop product ion libraries using a consistent
844 methodology so that PIDs can be compared directly from different studies. Consistent with the decades of previous research,
845 which includes measurements on PTR-MS instruments that use a drift tube for ionization, we observe E/N as a predictor of
846 the extent clustering or fragmentation product ions contribute to the PID of a VOC. Of particular importance for the instruments
847 in this study, is also the influence of ΔV_2 in creating “E/N-like effects” on PIDs and the BSQ RF voltage affecting PIDs through
848 mass-discrimination.

849

850 We demonstrate here that instrument tuning can affect PIDs, but tuning can also affect instrument sensitivity. We do not
851 discuss the relationship between instrument tuning, product ion formation, and instrument sensitivity here, but instead point
852 the reader to Li et al. (2024) for a detailed evaluation of this relationship relevant for Vocus PTR-ToF-MS instruments.
853 However, we note that specific instrument tuning properties explored here have implications for instrument sensitivity. For
854 instance, Li et al. (2024) showed that the H^+ adduct contribution to the PID and sensitivity for 1,3,5-trimethylbenzene did not
855 change appreciably with increasing E/N whereas the H^+ adduct contribution to the PID and sensitivity for hexanal (PID shown
856 here in Fig. 10) decreased with increasing E/N. This comparison demonstrates that VOCs susceptible to fragment ion formation
857 may show decreasing sensitivity to the H^+ adduct with increasing E/N. In addition to E/N we show that as the voltage difference
858 between the BSQ front and Skimmer (ΔV_2) increases this can increase fragmentation, and decrease water clustering, product
859 ion contributions to the PIDs (Fig. 5),

860

861 In another example, we demonstrated that higher BSQ voltages can filter out lower m/q ions and affect measured PIDs, but
862 another implication of higher BSQ voltages is that the sensitivity of the H^+ adduct for lower molecular weight species (e.g.,
863 formaldehyde, acetonitrile, formic acid, etc.) will also decrease. Interlaboratory comparisons focusing on constraining the
864 relationship between PIDs and instrument sensitivity would be informative for the development of standard tuning
865 configurations optimized for the measurement of specific VOCs or types of VOCs (e.g., aldehydes, aromatics, etc.).

867 Despite having similar operating conditions (i.e. similar E/N and BSQ voltage settings), PIDs measured across laboratories
868 showed considerable variability. Further, PIDs measured from the same instrument over time were not consistent. Our
869 observations support the conclusion that if a user configures the same model PTR-MS identically to an instrument in the
870 literature, they should not expect identical PIDs. Additionally, a user may expect different PIDs from the same instrument after
871 several months.

872
873 However, we also show that some of the variability in PIDs between instruments was explainable from qualitative arguments.
874 For example, Lab 6 operated with the highest E/N and showed the largest contributions of fragmentation and charge/hydride
875 transfer products to PIDs and small contributions from water clusters compared to the other labs. Qualitative arguments based
876 on E/N or BSQ voltage could not completely explain the variation in water clustering between labs. The quantitative constraints
877 on PIDs presented here could be improved with continued input of data from users to the H_3O^+ PID library (included here as
878 a supplemental document). Future work from our group at NIST will focus on integrating measurements of PIDs contained in
879 the existing PTR library from Pagonis et al. (2019) with the H_3O^+ PID library included here. We encourage users to continue
880 to contribute data for inclusion in the H_3O^+ PID library in continued efforts to understand PIDs and standardize methods of
881 PTR-MS measurements.

882 **5 Outlook**

883 All reagent ions used for chemical ionization mass spectrometry create unintended product ions that can present challenges
884 when identifying and quantifying VOCs. Continued work characterizing and constraining the impact of instrument operating
885 parameters and sampling methods on product ion generation is warranted to leverage the sensitivity, selectivity, and versatile
886 sampling capabilities that field-deployable chemical ionization mass spectrometers provide. PTR-MS users should be aware
887 that product ion generation (of not only fragments but also charge/hydride transfer and water clusters) occurs for most VOCs
888 to varying degrees. Additionally, the ambiguity created from product ion contributions to mass spectra measured from
889 chemically complex samples may create challenges to accurate identification and quantification of VOCs—particularly for
890 non-targeted analyses. Further characterization of PIDs across many PTR-MS instruments may be useful in constraining
891 interferences and decreasing the uncertainty from their influence on mass spectra.

892
893 There is a current interest to develop standardized methods of measurement using chemical ionization mass spectrometers.
894 Currently, no standard methods for sampling with PTR-MS or other chemical ionization instruments exists. Notable research
895 efforts towards standardization methods of PTR-MS measurements include the development of ion libraries (Pagonis et al.,
896 2019; Yáñez-Serrano et al., 2021), calibrations and standard reference materials (Worton et al., 2023; Jensen et al., 2023;
897 Sekimoto et al., 2017), data analysis methods (Holzinger, 2015; Cubison and Jimenez, 2015), and interlaboratory comparison

898 studies (Holzinger et al., 2019). Continued efforts, particularly in the form of coordinated interlaboratory comparison studies,
899 would be useful for the development of standard operational procedures and practices.

900 **Supplement**

901 Additional analyses of instrument configuration on PIDs are presented in the supplement. A spreadsheet containing the PID
902 data from the interlaboratory comparison (the “H₃O⁺ PID Library”) is included as a supplemental document and the most up-
903 to-date versions can be retrieved online (doi:10.18434/mds2-3582). Users wishing to submit data to this library can email the
904 corresponding author (michael.f.link@nist.gov) and a link to submit a data file will be provided. More details can be found in
905 the “ReadMe” tab of the supplemental H₃O⁺ PID Library.

906 **Competing Interests**

907 The contact author has declared that none of the authors has any competing interests.

908 **Acknowledgements**

909 We would like to acknowledge the National Research Council Research Associateship Program and Alfred P. Sloan
910 Foundation (G-2019-11404) for funding. This material is partially supported by the U.S. Department of Energy (DOE), Office
911 of Science, Office of Biological and Environmental Research, Atmospheric System Research (ASR) under Award No. DE-
912 SC0021985.

913 **Disclaimer**

914 Certain equipment, instruments, software, or materials, commercial or non-commercial, are identified in this paper in to specify
915 the experimental procedure adequately. Such identification is not intended to imply recommendation or endorsement of any
916 product or service by NIST, nor is it intended to imply that the materials or equipment identified are necessarily the best
917 available for the purpose.

918 **References**

919 Antony Joseph, M. J., McIntosh, D. G., Gibson, J. R., and Taylor, S.: Effects of the source gap on transmission efficiency of
920 a quadrupole mass spectrometer, *Rapid Communications in Mass Spectrometry*, 32, 677-685, 2018.
921 Arata, C., Misztal, P. K., Tian, Y., Lunderberg, D. M., Kristensen, K., Novoselac, A., Vance, M. E., Farmer, D. K., Nazaroff,
922 W. W., and Goldstein, A. H.: Volatile organic compound emissions during HOMEChem, *Indoor Air*, 31, 2099-2117, 2021.

923 Bielik, N., Correia, D., Rodrigues Crespo, K., Goujon-Ginglinger, C., and Mitova, M. I.: Pitfalls in the Detection of Volatiles
924 Associated with Heated Tobacco and e-Vapor Products When Using PTR-TOF-MS, *Journal of the American Society for Mass*
925 *Spectrometry*, 35, 1261-1271, 10.1021/jasms.4c00062, 2024.

926 Breitenlechner, M., Fischer, L., Hainer, M., Heinritzi, M., Curtius, J., and Hansel, A.: PTR3: An Instrument for Studying the
927 Lifecycle of Reactive Organic Carbon in the Atmosphere, *Analytical Chemistry*, 89, 5824-5831,
928 10.1021/acs.analchem.6b05110, 2017.

929 Brophy, P. and Farmer, D. K.: Clustering, methodology, and mechanistic insights into acetate chemical ionization using high-
930 resolution time-of-flight mass spectrometry, *Atmospheric Measurement Techniques*, 9, 3969-3986, 2016.

931 Buhr, K., van Ruth, S., and Delahunty, C.: Analysis of volatile flavour compounds by Proton Transfer Reaction-Mass
932 Spectrometry: fragmentation patterns and discrimination between isobaric and isomeric compounds, *International Journal of*
933 *Mass Spectrometry*, 221, 1-7, 2002.

934 Claflin, M. S., Pagonis, D., Finewax, Z., Handschy, A. V., Day, D. A., Brown, W. L., Jayne, J. T., Worsnop, D. R., Jimenez,
935 J. L., and Ziemann, P. J.: An in situ gas chromatograph with automatic detector switching between PTR-and EI-TOF-MS:
936 isomer-resolved measurements of indoor air, *Atmospheric Measurement Techniques*, 14, 133-152, 2021.

937 Coggon, M. M., Stockwell, C. E., Claflin, M. S., Pfannerstill, E. Y., Xu, L., Gilman, J. B., Marcantonio, J., Cao, C., Bates, K.,
938 and Gkatzelis, G. I.: Identifying and correcting interferences to PTR-ToF-MS measurements of isoprene and other urban
939 volatile organic compounds, *Atmospheric Measurement Techniques*, 17, 801-825, 2024.

940 Cubison, M. J. and Jimenez, J. L.: Statistical precision of the intensities retrieved from constrained fitting of overlapping peaks
941 in high-resolution mass spectra, *Atmospheric Measurement Techniques*, 8, 2333-2345, 10.5194/amt-8-2333-2015, 2015.

942 De Gouw, J. and Warneke, C.: Measurements of volatile organic compounds in the earth's atmosphere using proton-transfer-
943 reaction mass spectrometry, *Mass spectrometry reviews*, 26, 223-257, 2007.

944 De Gouw, J., Warneke, C., Karl, T., Eerdekens, G., Van der Veen, C., and Fall, R.: Sensitivity and specificity of atmospheric
945 trace gas detection by proton-transfer-reaction mass spectrometry, *International Journal of Mass Spectrometry*, 223, 365-382,
946 2003.

947 Demarcke, M., Amelynck, C., Schoon, N., Dhooghe, F., Rimetz-Planchon, J., Van Langenhove, H., and Dewulf, J.: Laboratory
948 studies in support of the detection of biogenic unsaturated alcohols by proton transfer reaction-mass spectrometry, *International*
949 *Journal of Mass Spectrometry*, 290, 14-21, 10.1016/j.ijms.2009.11.005, 2010.

950 Ditto, J. C., Crilley, L. R., Lao, M., Vandenboer, T. C., Abbatt, J. P. D., and Chan, A. W. H.: Indoor and outdoor air quality
951 impacts of cooking and cleaning emissions from a commercial kitchen, *Environmental Science: Processes & Impacts*, 25,
952 964-979, 10.1039/d2em00484d, 2023.

953 Ditto, J. C., Huynh, H. N., Yu, J., Link, M., Poppendieck, D., Claflin, M., Vance, M. E., Farmer, D., Chan, A., and Abbatt, J.:
954 Speciating volatile organic compounds in indoor air: using in-situ GC to interpret real-time PTR-MS signals, *Environmental*
955 *Science: Processes & Impacts*, 10.1039/d4em00602j, 2025.

956 Ernle, L., Wang, N., Bekö, G., Morrison, G., Wargocki, P., Weschler, C. J., and Williams, J.: Assessment of aldehyde
957 contributions to PTR-MS m/z 69.07 in indoor air measurements, *Environmental Science: Atmospheres*, 3, 1286-1295, 2023.

958 Gkatzelis, G. I., Coggon, M. M., Stockwell, C. E., Hornbrook, R. S., Allen, H., Apel, E. C., Bela, M. M., Blake, D. R.,
959 Bourgeois, I., and Brown, S. S.: Parameterizations of US wildfire and prescribed fire emission ratios and emission factors
960 based on FIREX-AQ aircraft measurements, *Atmospheric Chemistry and Physics*, 24, 929-956, 2024.

961 Hegen, O., Salazar Gómez, J. I., Schlägl, R., and Ruland, H.: The potential of NO^+ and $\text{O}_2^{\cdot+}$ in switchable reagent ion proton
962 transfer reaction time-of-flight mass spectrometry, *Mass Spectrometry Reviews*, 42, 1688-1726, 10.1002/mas.21770, 2023.

963 Heinritzi, M., Simon, M., Steiner, G., Wagner, A. C., Kürten, A., Hansel, A., and Curtius, J.: Characterization of the mass-
964 dependent transmission efficiency of a CIMS, *Atmospheric measurement techniques*, 9, 1449-1460, 2016.

965 Hodshire, A. L., Carter, E., Mattila, J. M., Ilacqua, V., Zambrana, J., Abbatt, J. P., Abeleira, A., Arata, C., DeCarlo, P. F., and
966 Goldstein, A. H.: Detailed Investigation of the Contribution of Gas-Phase Air Contaminants to Exposure Risk during Indoor
967 Activities, *Environmental science & technology*, 56, 12148-12157, 2022.

968 Holzinger, R.: PTRwid: A new widget tool for processing PTR-TOF-MS data, *Atmospheric Measurement Techniques*, 8,
969 3903-3922, 10.5194/amt-8-3903-2015, 2015.

970 Holzinger, R., Acton, W. J. F., Bloss, W. J., Breitenlechner, M., Crilley, L. R., Dusanter, S., Gonin, M., Gros, V., Keutsch, F.
971 N., and Kiendler-Scharr, A.: Validity and limitations of simple reaction kinetics to calculate concentrations of organic
972 compounds from ion counts in PTR-MS, *Atmospheric measurement techniques*, 12, 6193-6208, 2019.

973 Hopstock, K. S., Perraud, V., Dalton, A. B., Barletta, B., Meinardi, S., Weltman, R. M., Mirkhanian, M. A., Rakosi, K. J.,
974 Blake, D. R., Edwards, R. D., and Nizkorodov, S. A.: Chemical Analysis of Exhaled Vape Emissions: Unraveling the
975 Complexities of Humectant Fragmentation in a Human Trial Study, *Chemical Research in Toxicology*, 37, 1000-1010,
976 10.1021/acs.chemrestox.4c00088, 2024.

977 Jensen, A. R., Koss, A. R., Hales, R. B., and De Gouw, J. A.: Measurements of volatile organic compounds in ambient air by
978 gas-chromatography and real-time Vocus PTR-TOF-MS: calibrations, instrument background corrections, and introducing a
979 PTR Data Toolkit, *Atmospheric Measurement Techniques*, 16, 5261-5285, 10.5194/amt-16-5261-2023, 2023.

980 Joó, É., Dewulf, J., Demarcke, M., Amelynck, C., Schoon, N., Müller, J. F., Šimpraga, M., Steppe, K., and Van Langenhove,
981 H.: Quantification of interferences in PTR-MS measurements of monoterpene emissions from *Fagus sylvatica* L. using
982 simultaneous TD-GC-MS measurements, *International Journal of Mass Spectrometry*, 291, 90-95,
983 10.1016/j.ijms.2010.01.018, 2010.

984 Kari, E., Miettinen, P., Yli-Pirilä, P., Virtanen, A., and Faiola, C. L.: PTR-ToF-MS product ion distributions and humidity-
985 dependence of biogenic volatile organic compounds, *International Journal of Mass Spectrometry*, 430, 87-97,
986 10.1016/j.ijms.2018.05.003, 2018.

987 Kilgour, D. B., Novak, G. A., Claflin, M. S., Lerner, B. M., and Bertram, T. H.: Production of oxygenated volatile organic
988 compounds from the ozonolysis of coastal seawater, *Atmospheric Chemistry and Physics*, 24, 3729-3742, 10.5194/acp-24-
989 3729-2024, 2024.

990 Klein, F., Platt, S. M., Farren, N. J., Detournay, A., Bruns, E. A., Bozzetti, C., Daellenbach, K. R., Kilic, D., Kumar, N. K.,
991 and Pieber, S. M.: Characterization of gas-phase organics using proton transfer reaction time-of-flight mass spectrometry:
992 cooking emissions, *Environmental science & technology*, 50, 1243-1250, 2016.

993 Koss, A. R., Warneke, C., Yuan, B., Coggon, M. M., Veres, P. R., and de Gouw, J. A.: Evaluation of NO^+ reagent ion chemistry
994 for online measurements of atmospheric volatile organic compounds, *Atmospheric Measurement Techniques*, 9, 2909-2925,
995 2016.

996 Krechmer, J., Lopez-Hilfiker, F., Koss, A., Hutterli, M., Stoermer, C., Deming, B., Kimmel, J., Warneke, C., Holzinger, R.,
997 Jayne, J., Worsnop, D., Fuhrer, K., Gonin, M., and De Gouw, J.: Evaluation of a New Reagent-Ion Source and Focusing Ion-
998 Molecule Reactor for Use in Proton-Transfer-Reaction Mass Spectrometry, *Analytical Chemistry*, 90, 12011-12018,
999 10.1021/acs.analchem.8b02641, 2018.

1000 Li, F., Huang, D. D., Tian, L., Yuan, B., Tan, W., Zhu, L., Ye, P., Worsnop, D., Hoi, K. I., and Mok, K. M.: Response of
1001 protonated, adduct, and fragmented ions in Vocus proton-transfer-reaction time-of-flight mass spectrometer (PTR-ToF-MS),
1002 *Atmospheric Measurement Techniques*, 17, 2415-2427, 2024.

1003 Li, H., Almeida, T. G., Luo, Y., Zhao, J., Palm, B. B., Daub, C. D., Huang, W., Mohr, C., Krechmer, J. E., and Kurtén, T.:
1004 Fragmentation inside proton-transfer-reaction-based mass spectrometers limits the detection of ROOR and ROOH peroxides,
1005 *Atmospheric Measurement Techniques*, 15, 1811-1827, 2022.

1006 Link, M. F., Robertson, R. L., Shore, A., Hamadani, B. H., Cecelski, C. E., and Poppendieck, D. G.: Ozone generation and
1007 chemistry from 222 nm germicidal ultraviolet light in a fragrant restroom, *Environmental Science: Processes & Impacts*, 26,
1008 1090-1106, 2024.

1009 Liu, J., Jiang, J., Ding, X., Patra, S. S., Cross, J. N., Huang, C., Kumar, V., Price, P., Reidy, E. K., Tasoglou, A., Huber, H.,
1010 Stevens, P. S., Boor, B. E., and Jung, N.: Real-time evaluation of terpene emissions and exposures during the use of scented
1011 wax products in residential buildings with PTR-TOF-MS, *Building and Environment*, 255, 111314,
1012 10.1016/j.buildenv.2024.111314, 2024.

1013 Logue, J. M., McKone, T. E., Sherman, M. H., and Singer, B. C.: Hazard assessment of chemical air contaminants measured
1014 in residences, *Indoor Air*, 21, 92-109, 10.1111/j.1600-0668.2010.00683.x, 2011.

1015 Lopez-Hilfiker, F. D., Iyer, S., Mohr, C., Lee, B. H., D'Ambro, E. L., Kurtén, T., and Thornton, J. A.: Constraining the
1016 sensitivity of iodide adduct chemical ionization mass spectrometry to multifunctional organic molecules using the collision
1017 limit and thermodynamic stability of iodide ion adducts, *Atmospheric Measurement Techniques*, 9, 1505-1512, 2016.

1018 Materić, D., Lanza, M., Sulzer, P., Herbig, J., Bruhn, D., Gauci, V., Mason, N., and Turner, C.: Selective reagent ion-time of
1019 flight-mass spectrometry study of six common monoterpenes, *International Journal of Mass Spectrometry*, 421, 40-50,
1020 10.1016/j.ijms.2017.06.003, 2017.

1021 Mattila, J. M., Arata, C., Abeleira, A., Zhou, Y., Wang, C., Katz, E. F., Goldstein, A. H., Abbatt, J. P., DeCarlo, P. F., and
1022 Vance, M. E.: Contrasting Chemical Complexity and the Reactive Organic Carbon Budget of Indoor and Outdoor Air,
1023 Environmental Science & Technology, 56, 109-118, 2021.

1024 McCrumb, J. L. and Warneck, P.: On the mechanism of water cluster-ion formation in nitrogen, The Journal of Chemical
1025 Physics, 67, 5006-5011, 10.1063/1.434722, 1977.

1026 Misztal, P., Heal, M., Nemitz, E., and Cape, J.: Development of PTR-MS selectivity for structural isomers: Monoterpenes as
1027 a case study, International Journal of Mass Spectrometry, 310, 10-19, 2012.

1028 Molinier, B., Arata, C., Katz, E. F., Lunderberg, D. M., Ofodile, J., Singer, B. C., Nazaroff, W. W., and Goldstein, A. H.:
1029 Bedroom Concentrations and Emissions of Volatile Organic Compounds during Sleep, Environmental Science &
1030 Technology, 58, 7958-7967, 10.1021/acs.est.3c10841, 2024.

1031 Müller, M., Mikoviny, T., and Wisthaler, A.: Detector aging induced mass discrimination and non-linearity effects in PTR-
1032 ToF-MS, International Journal of Mass Spectrometry, 365-366, 93-97, 10.1016/j.ijms.2013.12.008, 2014.

1033 Nazaroff, W. W. and Weschler, C. J.: Methanol and ethanol in indoor environments, Indoor Environments, 1, 100049,
1034 10.1016/j.indenv.2024.100049, 2024.

1035 NIST: H₃O⁺ PTR-MS PID Library [dataset], doi:10.18434/mds2-3582, 2024.

1036 Pagonis, D., Sekimoto, K., and de Gouw, J.: A library of proton-transfer reactions of H₃O⁺ ions used for trace gas detection,
1037 Journal of the American Society for Mass Spectrometry, 30, 1330-1335, 2019.

1038 Reinecke, T., Leiminger, M., Jordan, A., Wisthaler, A., and Müller, M.: Ultrahigh Sensitivity PTR-MS Instrument with a Well-
1039 Defined Ion Chemistry, Analytical Chemistry, 95, 11879-11884, 10.1021/acs.analchem.3c02669, 2023.

1040 Seaman, V. Y., Bennett, D. H., and Cahill, T. M.: Origin, Occurrence, and Source Emission Rate of Acrolein in Residential
1041 Indoor Air, Environmental Science & Technology, 41, 6940-6946, 10.1021/es0707299, 2007.

1042 Sekimoto, K. and Koss, A. R.: Modern mass spectrometry in atmospheric sciences: Measurement of volatile organic
1043 compounds in the troposphere using proton-transfer-reaction mass spectrometry, Journal of Mass Spectrometry, 56, e4619,
1044 2021.

1045 Sekimoto, K., Li, S.-M., Yuan, B., Koss, A., Coggon, M., Warneke, C., and de Gouw, J.: Calculation of the sensitivity of
1046 proton-transfer-reaction mass spectrometry (PTR-MS) for organic trace gases using molecular properties, International Journal
1047 of Mass Spectrometry, 421, 71-94, 2017.

1048 Sheu, R., Stönnér, C., Ditto, J. C., Klüpfel, T., Williams, J., and Gentner, D. R.: Human transport of thirdhand tobacco smoke:
1049 A prominent source of hazardous air pollutants into indoor nonsmoking environments, Science Advances, 6, eaay4109,
1050 10.1126/sciadv.aay4109, 2020.

1051 Smith, D., McEwan, M. J., and Španěl, P.: Understanding Gas Phase Ion Chemistry Is the Key to Reliable Selected Ion Flow
1052 Tube-Mass Spectrometry Analyses, Analytical Chemistry, 92, 12750-12762, 10.1021/acs.analchem.0c03050, 2020.

1053 Španěl, P. and Smith, D.: SIFT studies of the reactions of H₃O⁺, NO⁺ and O₂⁺ with a series of alcohols, International Journal
1054 of Mass Spectrometry and Ion Processes, 167-168, 375-388, 10.1016/s0168-1176(97)00085-2, 1997.

1055 Španěl, P., Doren, J. M. V., and Smith, D.: A selected ion flow tube study of the reactions of H₃O⁺, NO⁺, and O₂⁺ with
1056 saturated and unsaturated aldehydes and subsequent hydration of the product ions, International Journal of Mass Spectrometry,
1057 213, 163-176, 10.1016/s1387-3806(01)00531-0, 2002.

1058 Tani, A.: Fragmentation and Reaction Rate Constants of Terpenoids Determined by Proton Transfer Reaction-mass
1059 Spectrometry, Environment Control in Biology, 51, 23-29, 10.2525/ecb.51.23, 2013.

1060 Vermeuel, M. P., Novak, G. A., Kilgour, D. B., Claflin, M. S., Lerner, B. M., Trowbridge, A. M., Thom, J., Cleary, P. A.,
1061 Desai, A. R., and Bertram, T. H.: Observations of biogenic volatile organic compounds over a mixed temperate forest during
1062 the summer to autumn transition, Atmospheric Chemistry and Physics, 23, 4123-4148, 2023.

1063 Wang, N., Müller, T., Ernle, L., Bekö, G., Wargoeki, P., and Williams, J.: How Does Personal Hygiene Influence Indoor Air
1064 Quality?, Environmental Science & Technology, 2024.

1065 Warneke, C., De Gouw, J. A., Kuster, W. C., Goldan, P. D., and Fall, R.: Validation of atmospheric VOC measurements by
1066 proton-transfer-reaction mass spectrometry using a gas-chromatographic preseparation method, Environmental science &
1067 technology, 37, 2494-2501, 2003.

1068 Worton, D. R., Moreno, S., O'Daly, K., and Holzinger, R.: Development of an International System of Units (SI)-traceable
1069 transmission curve reference material to improve the quantitation and comparability of proton-transfer-reaction mass-
1070 spectrometry measurements, Atmospheric Measurement Techniques, 16, 1061-1072, 10.5194/amt-16-1061-2023, 2023.

1071 Xu, L., Coggon, M. M., Stockwell, C. E., Gilman, J. B., Robinson, M. A., Breitenlechner, M., Lamplugh, A., Crounse, J. D.,
1072 Wennberg, P. O., Neuman, J. A., Novak, G. A., Veres, P. R., Brown, S. S., and Warneke, C.: Chemical ionization mass
1073 spectrometry utilizing ammonium ions (NH_4^+ CIMS) for measurements of organic compounds in the atmosphere, *Atmospheric*
1074 *Measurement Techniques*, 15, 7353-7373, 10.5194/amt-15-7353-2022, 2022.
1075 Yáñez-Serrano, A. M., Filella, I., Llusia, J., Gargallo-Garriga, A., Granda, V., Bourtsoukidis, E., Williams, J., Seco, R.,
1076 Cappellin, L., Werner, C., De Gouw, J., and Peñuelas, J.: GLOVOCS - Master compound assignment guide for proton transfer
1077 reaction mass spectrometry users, *Atmospheric Environment*, 244, 117929, 10.1016/j.atmosenv.2020.117929, 2021.
1078 Yuan, B., Koss, A. R., Warneke, C., Coggon, M., Sekimoto, K., and de Gouw, J. A.: Proton-transfer-reaction mass
1079 spectrometry: applications in atmospheric sciences, *Chemical reviews*, 117, 13187-13229, 2017.

1080